Reshape-then-Factorize: Communication-Efficient FL via Model-Agnostic Projection Optimization

Anonymous Author(s)
Affiliation
Address
email

Abstract

Federated learning (FL) enables collaborative model training across distributed clients without sharing sensitive data. However, communication overhead remains a significant bottleneck, particularly for large-scale models. Low-rank decomposition techniques address this by approximating each layer's weights or gradients with a product of low-rank matrices, thereby reducing the communication cost in FL. While effective, these methods are constrained by the layer's architecture and shapes, limiting their flexibility and performance. We propose *Model-Agnostic Projection Optimization* (MAPO), a novel method that reshapes and factorizes the full model gradient into a *fixed reconstruction matrix* and a *trainable projection vector*, avoiding layer-wise decomposition and architecture constraints. MAPO directly optimizes the projection in a randomly sampled subspace, with all clients generating the reconstruction matrix via a shared random seed, incurring no additional communication overhead for synchronization. By decoupling the gradient from architectural constraints through reshaping and enabling communication-free exploration of dynamic subspaces via seed sharing, MAPO provides a more flexible and efficient low-rank representation. Empirical results demonstrate the effectiveness of MAPO in various FL settings.

1 Introduction

Federated Learning (FL) is a distributed framework that enables model training across many clients without centralizing data. In each communication round, clients download a global model, update it using local data, and send modifications back to the server, which aggregates them (e.g., via FedAvg [1]). While this iterative process enables collaborative learning, frequent transmission of model updates incurs significant communication overhead, limiting FL application, particularly with large models or resource-constrained clients.

Communication-Efficient Federated Learning (CEFL) literature [2] proposes a vast range of strategies to reduce communication load. These methods are typically categorized into *sketched updates*, which compress the total model update after optimization (e.g., subsampling, quantization, random projection), and *structured updates*, which restrict the trainable parameters to a lower-dimensional subspace before optimization (e.g., random masks, weight-sharing, and low-rank decomposition) [3].

Low-rank decomposition is a widely used approximation technique that expresses model gradients or parameters as the product of low-rank matrices [4]. *Parameter decomposition* is particularly effective for Parameter-Efficient Fine-Tuning (PEFT), where auxiliary low-rank adaptation (LoRA) modules are added to each layer to reduce computation and storage overhead of full-model fine-tuning [5]. Although LoRA alleviates communication burdens in FL, constraining model parameters to a low-rank subspace can degrade performance. In contrast, *gradient decomposition* preserves full-rank model representations during inference and restricts only the gradients to a low-rank form during backpropagation [6–10]. A visual comparison is shown in Figure 1.

Submitted to 39th Conference on Neural Information Processing Systems (NeurIPS 2025). Do not distribute.

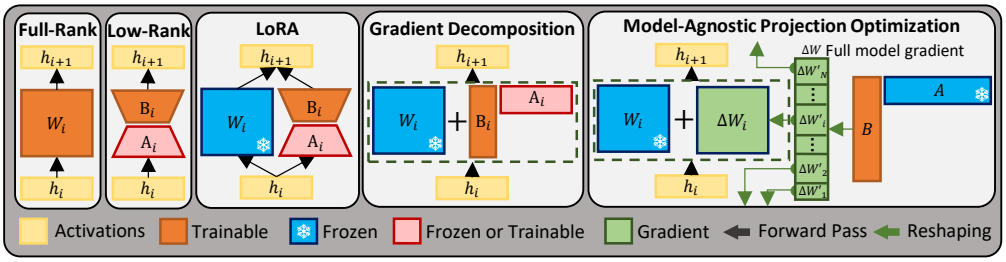

Figure 1: Comparison of various decomposition methods, from left: no decomposition, low-rank parameter decomposition, frozen model with low-rank adapter (LoRA), low-rank gradient decomposition, and MAPO.

Challenges. While CEFL methods for gradient decomposition [11–15], parameter decomposition [16–20], or LoRA variants [21–25] offer notable benefits, they face several key challenges: 1) The layer-wise decomposition that adheres to the structural constraints (e.g., fully connected or convolutional), requiring *architecture-dependent* implementation for each layer decomposition. 2) Given a decomposition $\Delta W_i \in \mathbb{R}^{d_1 \times d_2} \approx B_i A_i$, where $A_i \in \mathbb{R}^{r \times d_2}$ and $B_i \in \mathbb{R}^{d_1 \times r}$, the number of transmitted parameters is $\mathbf{C} = |A_i| + |B_i| = r(d_1 + d_2)$ for $r \in \mathbb{N}$, restricting the communication rate to multiples of $(d_1 + d_2)$, imposing a *rigid communication granularity* as $C \in (d_1 + d_2)\mathbb{N}$. 3) Given M number of clients and (A_i^j, B_i^j) denoting the low-rank decomposition of layer i from client j, averaging these low-rank matrices is *not equivalent to full-rank aggregation* as:

$$\frac{1}{M}(B_i^1 A_i^1 + B_i^2 A_i^2 + \cdots + B_i^M A_i^M) \neq \frac{1}{M}(B_i^1 + B_i^2 + \cdots + B_i^M)\frac{1}{M}(A_i^1 + A_i^2 + \cdots + A_i^M).$$

4) Although fixing all $\{A_i^j\}_{j=1}^M$ matrices to the same values can mitigate the aggregation problem and improve the communication granularity to $\mathbf{C} \in d_1\mathbb{N}$, as shown in FA-LoRA [21] and EvoFed [26], it restricts the model's ability to explore richer subspaces, often leading to *suboptimal solutions* [25]. Thus, we aim to answer the following key question:

How can we develop an architecture-independent model-wide decomposition that offers flexibility on communication rate, address the low-rank averaging problem, and suboptimality of freezing A?

Key Ideas. We propose a novel Model-Agnostic Projection Optimization (**MAPO**) that streamlines gradient projection and addresses its challenges while being computationally lighter than layer-wise methods. Our key ideas are described as follows:

(i) Firstly, MAPO reimagines low-rank gradient projection by treating the entire model gradient as a single matrix rather than layer-by-layer decomposition. It eliminates architecture-specific constraints by merging the flattened gradients of all layers, constructing the *universal gradient vector* $\Delta W \in \mathbb{R}^d$.

(ii) Secondly, given any communication budget k, MAPO pads ΔW with zeros so the length becomes divisible by k. Afterwards, padded ΔW will be reshaped to $\Delta W' \in \mathbb{R}^{k \times \lceil d/k \rceil}$ which further can be decomposed it into a $A \in \mathbb{R}^{1 \times \lceil d/k \rceil}$ and $B \in \mathbb{R}^{k \times 1}$ matrices, as $\Delta W' = BA$.

(iii) Lastly, instead of relying on a fixed A, MAPO explores new subspaces in each federated round through reinitialization of A, mitigating the risk of suboptimal convergence. Synchronization of A is achieved efficiently via a shared seed, removing the need to transmit A.

Summary of Contributions. By integrating **(i)** model-level decomposition, **(ii)** flexible communication rate, and **(iii)** subspace exploration, MAPO offers a flexible trade-off between communication cost and performance while remaining more efficient than low-rank decomposition methods. Figure 3 illustrates the distinction between MAPO and other paradigms. Our main contributions are:

- We introduce model-agnostic optimization of gradient projections that enhances communication and computation efficiency, boosts performance through exploration, and offers more flexibility in balancing communication and error rate.
- We provide theoretical analysis for MAPO convergence behavior, and establish its computation efficiency compared to layer-wise factorization with the same communication and error rates.
- We conduct extensive experiments across diverse datasets, model architectures, and baselines, demonstrating that MAPO surpasses existing methods in full training and fine-tuning scenarios.

2 Background and Related Works

In this section, we review key CEFL approaches in relation to MAPO. We begin with sketched update techniques that project model updates into subspaces, outlining their limitations. Then, we examine structured update methods, particularly projection optimization, highlighting the unique opportunities and challenges introduced by operating within a fixed subspace.

2.1 Sketched update vs. Structured update

Sketched update includes techniques such as sparsification [3], quantization [27–33], gradient subspace projection [34–36], and random subspace projection [26, 37]. They aim to compress the information in the update vector $\Delta W \in \mathbb{R}^d$ defined as the difference between the locally optimized and the global model $\Delta W = W^* - W_g$, where W^* can be the result of multiple local epochs.

The subspace projection process [37–40] defines a random matrix $A \in \mathbb{R}^{p \times d}$, and finds the projection vector $B \in \mathbb{R}^p$, which minimizes the reconstruction error $\|\Delta W - BA\|_2$, where d denotes the total number of model parameters and $p \ll d$ is compressed length:

$$B^* = \arg\min_{B \in \mathbb{R}^p} \|\Delta W - BA\|_2 \quad ; \quad B^* \approx \Delta W \mathbf{A}^\top (\mathbf{A}\mathbf{A}^\top)^{-1}.$$

As the matrix A is considerably large ($p \times d$), various methods propose novel designs for A to adapt it for large-scale models. Notably, defining A as a subset of seen gradient vectors results in a significantly lower rank of A suffices for an effective projection [34–36]. More recently, EvoFed [26] utilizes evolutionary strategies to evolve A, improving its representation and efficiency.

Sketching Limitations. Although sketched methods benefit from a full-rank training, their shortcoming is blindness to the loss surface $\mathcal{L}(W; \mathcal{D})$ and alternative solutions besides ΔW that can be reconstructed from the projection subspace. They typically perform well, given a sufficient communication budget, but as the compression rate increases, the reconstruction of the projection vector ends up far off from ΔW. In contrast, subspace optimization directly finds the steepest direction within the subspace, leading to a more effective reduction in loss. Figure 2 presents an example of centralized MNIST training, illustrating the performance degradation of sketched update techniques such as EvoFed [26] and Top-k Sparsification [3] compared to MAPO. As sparsity increases, MAPO continues to converge, even having 2 or 4 trainable parameters out of 11,274.

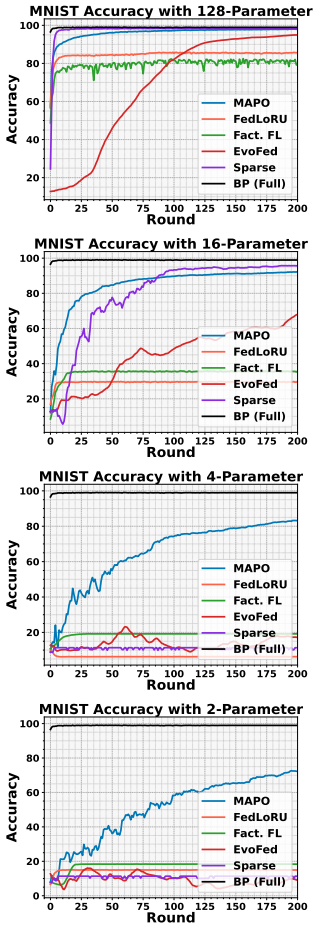

Figure 2: MNIST performance for varying trainable parameters.

Structured update techniques reduce the number of trainable parameters and communication cost by constraining the weights or gradients to a low-rank subspace by structural modification such as pruning [41–44], weight–sharing [45–47], low-rank gradient [11–15], and parameter decomposition [16–20], including LoRA and its variants [5, 21–24]. Although parameter decomposition techniques reduce the model size and representation, resulting in subpar performance for general training, as shown in Figure 2 for Factorized-FL [18]. Therefore, CEFL generally adopts a gradient decomposition direction. In particular, gradient decomposition methods with freezing A, also known as *projection optimization*, remain popular owing to strong theoretical foundations, reduced communication, and hardware friendliness [6–10].

Prior works on gradient decomposition relied on each layer's shape and architecture, producing a unique A_i and B_i matrices for each layer, limiting the feasibility of sharing a projection matrix A across layers. MAPO overcomes this limitation by evenly partitioning the whole model gradient vector $\Delta W \in \mathbb{R}^d$ into k segments $\{\Delta W'_i\}_{i=1}^k \in \mathbb{R}^{k \times \lceil d/k \rceil}$, allowing the use of a shared random reconstruction matrix $A \in \mathbb{R}^{1 \times \lceil d/k \rceil}$ across all partitions, maintaining the benefits of model-wide projection while substantially reducing memory costs.

2.2 Parameter-efficiency vs. Communication-efficiency

Despite their apparent similarities, parameter decomposition and gradient decomposition methods differ fundamentally in assumptions and objectives. Parameter decomposition directly imposes a low-rank structure on the model parameters, effectively replacing the original model with a compressed version. Although this reduces the total number of parameters and computational overhead, it still requires transmitting all parameters at each communication round, resulting in no relative reduction in communication per parameter. In contrast, gradient decomposition methods maintain the original

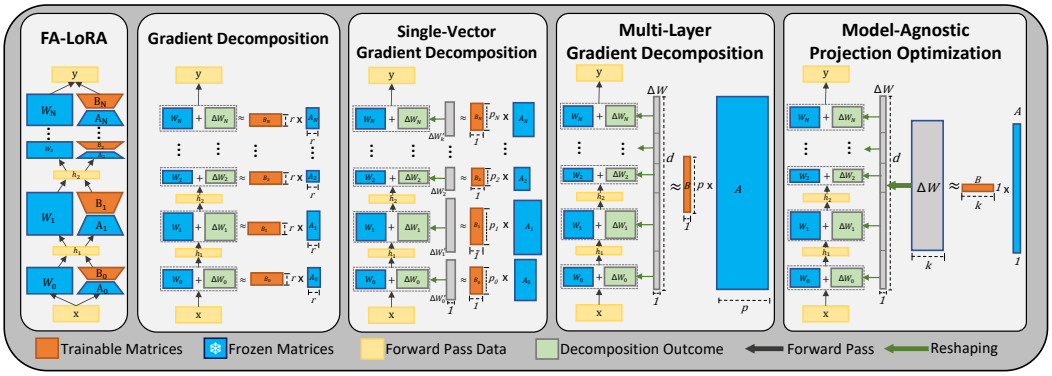

Figure 3: Step-by-Step illustration of methodology based on propositions, demonstrating how each step will contribute to designing MAPO factorization and differing from LoRA architecture.

model architecture and computational complexity but substantially reduce communication overhead by transmitting compressed updates that are significantly smaller than the full model.

In this work, to ensure a fair assessment of communication efficiency, we evaluate MAPO against gradient-based compression baselines under consistent model architectures. Additional experiments with parameter decomposition and LoRA-based methods are provided in Appendices B and C for completeness. Key methodological distinctions among related works are summarized in Table 1.

Table 1: Summary of CEFL methods and objectives. The column "Comm. Flex" indicates support for arbitrary bitrates, and "Agg. Eq." denotes equivalence between low-rank and full-rank averaging.

Method	Scope	Target	Full-rank Inference	Agg. Eq.	PEFT	Fixed Subspace	Arch-Agnostic	Comm Flex	Personalized FL
Sparsification [3]	Model	Update	✓	✓	✗	✗	✓	✓	✗
Quantization [32]	Model	Update	✓	✓	✗	✗	✓	✓	✗
EvoFed [26]	Model	Update	✓	✓	✗	✓	✓	✓	✗
Factorized-FL [18]	Layer	Parameter	✗	✗	✗	✗	✗	✗	✓
LoRA [5]	Layer	Adapter	✗	✗	✓	✗	✗	✗	✗
FA-LoRA [21]	Layer	Adapter	✗	✓	✓	✓	✗	✗	✗
SA-LoRA [25]	Layer	Adapter	✗	✗	✓	✗	✗	✗	✓
FedLoRU [13]	Layer	Gradient	✓	✓	✗	✓	✗	✗	✗
MAPO (Ours)	Model	Gradient	✓	✓	✗	✓	✓	✓	✗

3 Proposed Method

In this section, we introduce MAPO and its application in FL. We first present the MAPO factorization technique and discuss its key properties regarding communication efficiency and error rate. Subsequently, we detail how MAPO can be effectively integrated into the FL training process.

3.1 Model-Agnostic Projection Optimization (MAPO)

MAPO Description. MAPO performs a black-box, model-agnostic factorization of the global model gradient $\Delta W \in \mathbb{R}^d$, avoiding architecture-specific constraints and enabling continuous subspace exploration during optimization. Specifically, MAPO partitions ΔW into k segments $\{\Delta W'_i\}_{i=1}^{k} \in \mathbb{R}^{k \times \lceil d/k \rceil}$ and employs a shared random reconstruction matrix $A \in \mathbb{R}^{1 \times \lceil d/k \rceil}$ across all partitions. This design preserves model-wide projection benefits while substantially reducing memory overhead. As illustrated in Figure 1, MAPO reshapes the universal gradient $\Delta W \in \mathbb{R}^{d \times 1}$ into $\Delta W' \in \mathbb{R}^{k \times \lceil d/k \rceil}$, which is then decomposed into a reconstruction vector A and a projection vector $B \in \mathbb{R}^{k \times 1}$. Figure 3 shows a step-by-step visualization analogous to Theorems 3.4 to 3.6.

MAPO Properties. MAPO aims to construct an expressive subspace, enabling a small B to encode sufficient information for updating the model efficiently. First, we formally define the concepts of communication overhead rate and reconstruction error rate in the context of matrix factorization in Theorems 3.2 and 3.3. Using these definitions, Theorem 3.4 establishes that reshaping a single layer preserves both the factorization error and communication rates. Extending this, Theorem 3.5 demonstrates that vectorizing multiple layers into a single matrix similarly maintains these properties. Finally, this leads to the proof of Theorem 3.6, which introduces a computationally and communication-efficient, model-agnostic factorization method as an alternative to traditional layer-wise gradient projection techniques. Appendix G presents the formal proofs.

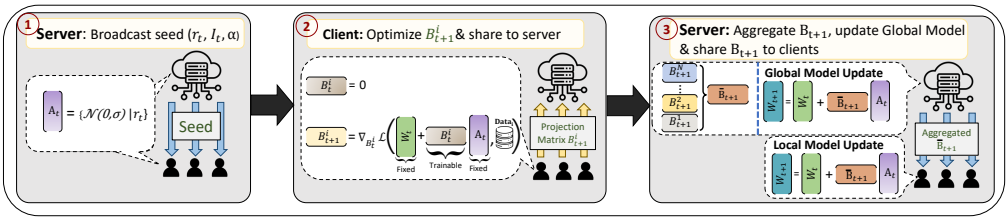

Figure 4: Application of MAPO to communication-efficient FL.

Assumption 3.1 (Gaussian Matrices are Full Rank). Let $A \in \mathbb{R}^{m\times n}$ be a random matrix with entries drawn independently from a Gaussian distribution $\mathcal{N}(0, \sigma^2)$. Then, A is almost surely of full rank, i.e., $\text{rank}(A) = \min(m, n)$, as the probability of A being rank deficient is zero. This result follows from standard properties of random matrices [48, 49].

Definition 3.2 (Communication Overhead Rate). Let $\Delta W_i \in \mathbb{R}^{d_1\times d_2}$ be the update matrix of a model. Suppose the factorization of ΔW_i as $\Delta W_i = B_i A_i$, where $A_i \in \mathbb{R}^{q\times d_2}$ is a fixed random matrix and $B_i \in \mathbb{R}^{d_1\times q}$ is a trainable matrix with $q \leq \min(d_1, d_2)$ being the factorization rank. The **communication overhead rate** CO_{rate} is defined as the ratio of the size of B_i to the size of ΔW:

$$\text{CO}_{rate} = \frac{\text{size}(B_i)}{\text{size}(\Delta W_i)} = \frac{q}{d_2}.$$

Definition 3.3 (Reconstruction Error Rate). Using the same factorization as Theorem 3.2, the *reconstruction error rate* is the expected ratio of the reconstruction error to the original model update. Given full-rank random reconstruction (Theorem 3.1), it is expressed as:

$$\frac{\mathbb{E}_{A_i}\left[\|\Delta W_i - B_i A_i\|_2^2\right]}{\|\Delta W_i\|_2^2} = 1 - \frac{q}{d_2}.$$

Proposition 3.4 (Single-Vector Factorization). *Let ΔW_i, A_i, and B_i be factorizations of a single layer of the network as in Theorem 3.2. By reshaping ΔW_i into $\Delta W'_i \in \mathbb{R}^{1\times d_1 d_2}$ the factorization of $\Delta W'_i = B'_i A'_i$ where $A'_i \in \mathbb{R}^{p\times d_1 d_2}$ and $B'_i \in \mathbb{R}^{1\times p}$ can achieve the same **reconstruction error** and **communication overhead** to the conventional factorization of ΔW_i when $p = qd_1$.*

Proposition 3.5 (Multi-Layer Factorization). *Let ΔW_i, A_i, and B_i be **single-vector factorization** of i-th layer of the N-layered network as in Theorem 3.4. By concatenating the reshaped weights ΔW_i into $\Delta W' \in \mathbb{R}^{1\times d}$, where $d = \sum_{i=1}^{N} d_1^i d_2^i$. The factorization of $\Delta W' = B'A'$ where $A' \in \mathbb{R}^{p\times d}$ and $B' \in \mathbb{R}^{1\times p}$ can achieve the same **reconstruction error** and **communication overhead** to the single-vector factorization applied to each ΔW_i when $p = Nq$.*

Proposition 3.6 (MAPO Factorization). *Let ΔW, A, B, and rank p be a multi-layer factorization of a network as defined in Theorem 3.5. By reshaping $\Delta W \in \mathbb{R}^{1\times d}$ into $\Delta W' \in \mathbb{R}^{k\times\lceil d/k\rceil}$, and the factorization of $\Delta W' = B'A'$ where $A' \in \mathbb{R}^{1\times\lceil d/k\rceil}$ and $B' \in \mathbb{R}^{k\times 1}$, we can achieve the same **reconstruction error** and **communication overhead** to the multi-layer factorization of ΔW when $k = p$, while reducing the memory by a factor of k^2.*

3.2 Application to Communication-Efficient Federated Learning

This subsection explains how our method, outlined in Section 3.1, is utilized in FL. The procedure pseudo-code is provided in Algorithm 1, and visualized in Figure 4.

Matrix Construction and Broadcasting. To ensure consistency across the network, the server and all clients start from an identical condition at each round. We guarantee identical model parameters W_t and reconstruction matrix A_t by broadcasting a random seed r_t and the aggregated projection vector $\overline{B}_t$ at the beginning of round t. The initial aggregated projection vector is set to $\overline{B}_0 = \mathbf{0}$.

In the first round ($t = 0$), all clients and the server initialize the model W^0 using the same seed. The reconstruction matrix $A^0 \in \mathbb{R}^{1\times\lceil d/k\rceil}$ is drawn from Gaussian $A^0 \sim \mathcal{N}(0, I)$, and the client j's projection vector $B^{0,j} \in \mathbb{R}^{k\times 1}$ is set to 0 for all $1 \leq j \leq M$, where M is the total number of clients.

In subsequent rounds ($t \geq 1$), clients update their local model W^t using the previous round's matrix A^{t-1}, the model parameters W^{t-1}, and the broadcasted projection vector $\overline{B}^t$ as follows:

$$W^t = W^{t-1} + \mathbf{vec}(\overline{B}^t A^{t-1})_{[0:d]}, \tag{1}$$

where $\mathbf{vec}(\cdot)$ and $(\cdot)_{[0:d]}$ denotes vectorization and truncating to the first d elements. Clients then regenerate $A^t \sim \mathcal{N}(0, I)$ using the seed r^t and reset $B^{t,j} \leftarrow \mathbf{0}$, ensuring A^t and W^t synchronization.

Algorithm 1: Federated Learning with MAPO

Input : Initial random seed r^0, global model W^0, reconstruction matrix A^0, projection vector $\overline{B}^0$
Output : Final global model W^T

Initialize all clients and server with the same seed r^0;
Initialize $W^0 \in \mathbb{R}^d$, $A^0 \in \mathbb{R}^{1\times\lceil d/k\rceil}$, $\overline{B}^0 \leftarrow \mathbf{0} \in \mathbb{R}^{k\times 1}$;
for each communication round $t = 1, \ldots, T-1$ **do**
  Server: Broadcast $\overline{B}^{t-1}$ and seed r^{t-1} to all clients;
  for each **Client** $j = 1, \ldots, M$ (in parallel) **do**
    Receive $\overline{B}^{t-1}$ and r^{t-1};
    Update local model: $W^t \leftarrow W^{t-1} + \mathbf{vec}(\overline{B}^t A^{t-1})[0:d]$;
    Re-generate $A^t = \mathcal{N}(0, \sigma^2 I_d)\big|r^{t-1}$;
    Initialize $B^{t,j} \leftarrow \mathbf{0} \in \mathbb{R}^{k\times 1}$;
    for each local epoch $e = 1, \ldots, E$ **do**
      Compute gradient: $\nabla B^{t,j} \leftarrow \nabla_{B^{t,j}} \mathcal{L}^j(W^t + \mathbf{vec}(B^{t,j} A^{t-1})[0:d], \mathcal{D}^j)$;
      Update projection vector: $\hat{B}^{t,j} \leftarrow B^{t,j} - \eta \nabla B^{t,j}$;
      Set $B^{t,j} \leftarrow \hat{B}^{t,j}$;
    end
    Send $\hat{B}^{t,j}$ to the server;
  end
  Server:
  Re-generate $A^t = \mathcal{N}(0, \sigma^2 I_d)\big|r^{t-1}$;
  Aggregate: $\overline{B}^t \leftarrow \frac{1}{S}\sum_{j=1}^M b_j \hat{B}^{t,j}$, where $S = \sum_j b_j$;
  Update global model: $W^{t+1} \leftarrow W^t + \mathbf{vec}(\overline{B}^t A^{t-1})[0:d]$;
  Generate new seed r^t (e.g., $r^t = \text{hash}(r^{t-1})$);
end
return W^T;

Local Projection Optimization. This step optimizes the projection $\hat{B}^{t,j}$ to minimizes the client loss $\mathcal{L}(W^t + \mathbf{vec}(B^{t,j}A^{t-1})_{[0:d]}, \mathcal{D}^j)$, where $\mathcal{D}^j$ denotes client j's local dataset, and model weights are derived as $W^t + \mathbf{vec}(B^{t,j}A^t)_{[0:d]}$ given the random matrix A^t.

At each communication round $t \geq 1$, after initializing A_t and $B^{t,j}$, clients perform local training to optimize $B^{t,j}$ using their local data $\mathcal{D}^j$. The gradient of the projection vector is computed as:

$$\nabla B^{t,j} = \nabla_{B^{t,j}} \mathcal{L}^j(W^t + \mathbf{vec}(B^{t,j}A^{t-1})_{[0:d]}) \quad \textbf{for} \quad \mathcal{L}^j(W) = \frac{1}{|\mathcal{D}^j|}\sum_{x\in\mathcal{D}^j} \ell(W, x). \tag{2}$$

where $\ell(W, x)$ is the loss function (e.g., cross-entropy loss) given model W and data point x. Therefore, given the learning rate η, only the projection $\hat{B}^{t,j}$ is updated using gradient descent as:

$$\hat{B}^{t,j} \leftarrow B^{t,j} - \eta \nabla B^{t,j}, \tag{3}$$

After optimization, clients send their optimized projection vector $\hat{B}^{t,j}$ to the server. The low dimensionality of $\hat{B}^{t,j}$ compared to W^t results in communication efficiency.

Server-Side Aggregation and Global Model Update. Upon receiving the projection vectors $\hat{B}^{t,j}$ and their corresponding weights $b^j = |D^j|$ (e.g., batch sizes or number of local samples) from the clients, the server aggregates them to form the global projection vector:

$$\overline{B}^t = \frac{1}{S}\sum_{j=1}^M b^j \hat{B}^{t,j}, \quad \text{for} \quad S = \sum_{j=1}^M b_j \tag{4}$$

This weighted averaging captures the collective contribution of all clients, proportional to their data sizes. The server then broadcasts the aggregated projection vector $\overline{B}^t$ to all clients. After receiving $\overline{B}^t$, the server and all clients update their local models using the reconstruction matrix A^t and the aggregated projection vector $\overline{B}^t$ as:

$$W^{t+1} = W^t + \mathbf{vec}(\overline{B}^t A^{t-1})_{[0:d]}. \tag{5}$$

This update integrates the clients' optimized directions into their local models and ensures synchronization across the network. This process is repeated until the global model converges.

Table 2: Summary of datasets and models used in our experiments.

Dataset	Client Distribution	Train/Test	# Classes	Model	# Parameters
MNIST [50]	Non-IID (2 classes)	60K / 10K	10	CNN - 2 Layers	11,274
FMNIST [51]	Non-IID (2 classes)	60K / 10K	10	CNN - 2 Layers	11,274
CIFAR-10 [52]	Non-IID (2 classes)	50K / 10K	10	CNN - 4 Layers	1,146,634
CIFAR-100 [52]	Non-IID (10 classes)	50K / 10K	100	WideResNet 16d4w	2,854,420
TinyImageNet [53]	Non-IID (10 classes)	100K / 10K	200	WideResNet 16d4w	2,880,120
Shakespeare [54]	Distributed by Roles	14K / 2K	65	LSTM	814,957
Sentiment140 [54]	Distributed by Users	1.4M / 200K	2	Transformer	2,221,570
GLUE Tasks [55]	Non-IID	*differ per task*	*differ per task*	RoBERTa-Large	357,199,876

4 Convergence Analysis

We analyze the convergence behavior of FL with MAPO.

Assumption 4.1. For each j, $\mathcal{L}^j(v)$ is β-smooth, i.e., $\left\|\nabla\mathcal{L}^j(u)-\nabla\mathcal{L}^j(v)\right\| \leq \beta\|u-v\|$ for any u, v.

Assumption 4.2. Variance of the stochastic gradient of D^j is bounded for each client j, i.e.,

$$\mathbb{E}\Big[\Big\|\nabla\mathcal{L}^j(W) - \widetilde{\nabla}\mathcal{L}^j(W)\Big\|^2\Big] \leq \sigma_l^2$$

Theorem 4.3. *Let the learning rate satisfy $\eta_t \leq \frac{1-4\epsilon}{4\beta(1+\epsilon)}$. Then, the algorithm achieves the bound:*

$$\frac{1}{4H_T}\sum_{t=0}^{T-1}\eta_t\mathbb{E}\left[\left\|\nabla\mathcal{L}(W^t)\right\|^2\right] \leq \frac{\mathbb{E}\left[\mathcal{L}(W^0)\right]-\mathcal{L}^*}{H^T} + 2(\epsilon+\beta+\beta\epsilon)\sigma_l^2\frac{1}{H^T}\sum_{t=0}^{T-1}\eta_t^2,$$

where $H_T = \sum_{t=0}^{T-1}\eta_t$, ϵ is JL Lemma distortion parameter, and $\mathcal{L}^*$ is the minimum value of $\mathcal{L}(W)$.

With a decreasing learning rate satisfying $\sum_{t=0}^{\infty}\eta_t \to \infty$, $\sum_{t=0}^{\infty}\eta_t^2 < \infty$ ($\eta_t = \frac{\eta_0}{t+c}$ for some constants $\eta_0 > 0$, $c > 0$), the term $H_T = \sum_{t=0}^{T-1}\eta_t$ grows unbounded, while the weighted sum $\sum_{t=0}^{T-1}\eta_t^2$ remains finite. Therefore, the right-hand side of Theorem 4.3's bound satisfies:

$$\frac{\mathbb{E}[\mathcal{L}(W^0)]-\mathcal{L}^*}{H_T} \to 0, \quad \frac{1}{H_T}\sum_{t=0}^{T-1}\eta_t^2 \to 0 \quad \text{as} \quad T\to\infty.$$

Thus, confirming convergence to a stationary point, as the gradient norm average satisfies:

$$\frac{1}{H_T}\sum_{t=0}^{T-1}\eta_t\mathbb{E}\big[\|\nabla\mathcal{L}(W^t)\|^2\big] \to 0,$$

As shown above, the convergence bound is influenced by the factor $\epsilon+\beta+\beta\epsilon$. In particular, the bound becomes tightest and achieves the highest communication efficiency when there is no reconstruction error, i.e., when $\epsilon = 0$. The complete proof of Theorem 4.3 is located in Appendix H.

5 Experimental Setup

We evaluate MAPO across diverse model architectures, tasks, and baselines. The benchmarks span five image classification datasets—MNIST [50], FMNIST [51], CIFAR-10, CIFAR-100 [52], and TinyImageNet [53]—as well as sequential tasks, including next-character prediction on Shakespeare and sentiment analysis on Sentiment140, both drawn from the LEAF benchmark suite [54], tailored for FL. Additionally, we evaluate MAPO as a fine-tuning method, alongside LoRA baselines on various GLUE [55] tasks, highlighting the communication and computation efficiency in Appendix B. The dataset specifications and corresponding model architectures are summarized in Table 2, highlighting MAPO's adaptability across varying data modalities, model scales, and application domains.

Non-IID Distribution. To simulate realistic FL conditions, we partition the training datasets in a non-IID manner across 100 clients. For image classification and GLUE tasks, each client is assigned a distinct subset of classes. For LEAF tasks, we follow the natural user-based partitioning, where individual Shakespearean roles and Twitter users correspond to separate clients.

Model Architectures. We evaluate MAPO across diverse architectures of varying complexity, including CNNs (2-layer for MNIST and FMNIST; 4-layer for CIFAR-10), WideResNet (width 4, depth 16) for CIFAR-100 and TinyImageNet, LSTM for next-character prediction, Transformer for sentiment analysis, and RoBERTa for GLUE tasks. Detailed architecture specifications and hyperparameters are in Appendix D.

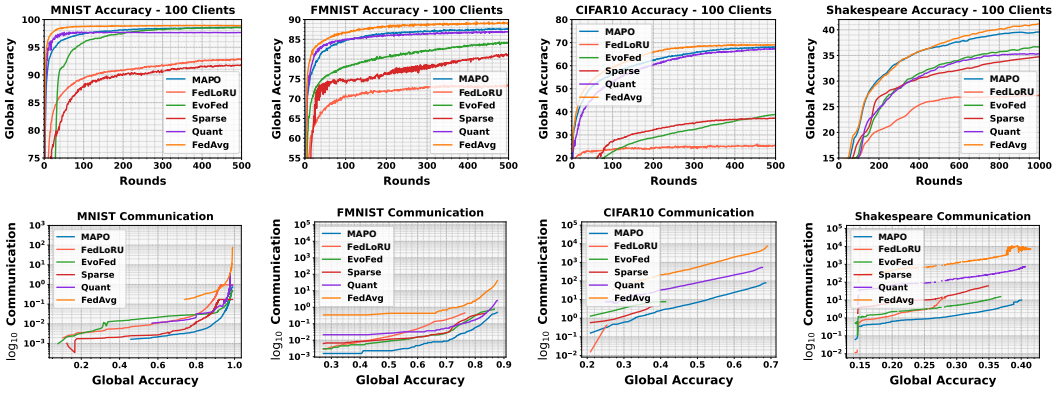

(a) MNIST (b) FMNIST (c) CIFAR-10 (d) Shakespeare

Figure 5: **Performance comparison** of all methods on MNIST, FMNIST, CIFAR-10, and Shakespeare datasets. The top row shows the accuracy, while the bottom row illustrates the communication cost per accuracy.

Table 3: Summary of maximum accuracy (%) and communication cost (% relative to FedAvg). Accuracy values report mean (±std) over 3 runs, estimated from observed variance.

	MNIST		FMNIST		CIFAR-10		CIFAR-100		Shakespeare		Sent140		TinyImageNet	
Method	Com.	Acc.	Com.	Acc.	Com.	Acc.	Com.	Acc.	Com.	Acc.	Com.	Acc.	Com.	Acc.
FedAvg	100	98.9 (±0.1)	100	89.2 (±0.2)	100	69.0 (±0.2)	100	43.47 (±0.3)	100	41.86 (±0.3)	100	74.90 (±0.3)	100	36.48 (±0.4)
Sparse	15.3	92.1 (±0.4)	24.1	81.1 (±0.4)	2.7	37.15 (±0.5)	1.20	33.72 (±0.5)	1.73	34.86 (±0.4)	1.93	74.21 (±0.3)	1.32	25.34 (±0.5)
Quantize	31.3	97.6 (±0.2)	24.1	87.1 (±0.3)	15.2	67.40 (±0.3)	6.10	40.05 (±0.4)	10.11	35.45 (±0.4)	13.85	73.70 (±0.3)	8.75	34.47 (±0.4)
EvoFed	9.40	98.5 (±0.2)	7.60	84.7 (±0.3)	3.4	39.50 (±0.4)	20.4	37.62 (±0.4)	0.23	36.76 (±0.3)	0.40	70.50 (±0.3)	1.85	15.40 (±0.5)
FedLoRU	30.2	93.8 (±0.4)	17.9	74.1 (±0.5)	1.7	23.52 (±0.5)	1.20	19.10 (±0.5)	1.67	28.07 (±0.5)	1.30	66.61 (±0.4)	1.27	7.31 (±0.5)
MAPO	**2.95**	**98.6 (±0.1)**	**3.10**	**88.0 (±0.2)**	**1.20**	**68.3 (±0.2)**	**0.91**	**40.16 (±0.3)**	**0.13**	**39.96 (±0.3)**	**0.19**	**74.50 (±0.2)**	**0.97**	**35.22 (±0.3)**

Baselines. We compare MAPO against multiple baselines, including standard compression methods with Top=k subsampling (Sparse) [3], and quantization (Quant) [32]. Additionally, we evaluate MAPO against EvoFed [26], a state-of-the-art gradient compression, and FedLoRU [13], a representative gradient projection approach. Subsampling and quantization serve as references to establish MAPO's performance compared to conventional compression techniques. EvoFed provides a strong comparison to demonstrate the effectiveness of MAPO's subspace optimization relative to methods applying compression post-optimization. FedLoRU allows us to highlight MAPO's dynamic subspace exploration and its benefits over static layer-wise gradient projections. Results comparing MAPO with additional parameter-factorization (Factorized-FL [18]) and adapter-based fine-tuning baselines (LoRA [5], FA-LoRA [21], and SA-LoRA [25]) are included in Appendices B and C.

Federated Learning Setting. In each training round, 10% of the clients are randomly selected to participate. Selected clients train locally in parallel and transmit their updates to the central server, which aggregates these updates and redistributes the resulting global model back to the clients. Model performance is evaluated centrally using the test dataset at the server.

6 Results and Discussions

We now discuss our experimental results in detail and provide insights into MAPO's performance. Figure 5 (top row) shows the accuracy of MAPO compared to multiple baseline methods across various datasets. MAPO consistently outperforms all other methods and achieves accuracy comparable to FedAvg, despite transmitting only a fraction of the parameters. This improvement results from MAPO's dynamic subspace optimization, which promotes effective exploration and efficient use of the communication budget to minimize the loss function directly. Additionally, Figure 5 (bottom row) illustrates the minimal communication cost required by each method to reach a given accuracy level, highlighting MAPO's significantly lower communication demands (logarithmic scale on the y-axis). Additional results on CIFAR-100, TinyImageNet, and Sentiment140 are presented in Appendix A.

Table 3 summarizes experimental results by comparing the maximum accuracy of each baseline and their communication cost relative to FedAvg. To ensure fair comparison, communication costs are reported as the percentage required to reach the accuracy of the worst-performing baseline. MAPO consistently achieves competitive accuracy with significantly lower communication overhead. Specifically, on MNIST and FMNIST, MAPO achieves 99.6% and 98.6% of FedAvg's accuracy, respectively, using only 3% of FedAvg's communication cost. For CIFAR-10, CIFAR-100, and TinyImageNet, MAPO attains 98.9%, 92.4%, and 96.5% of FedAvg accuracy, respectively, while

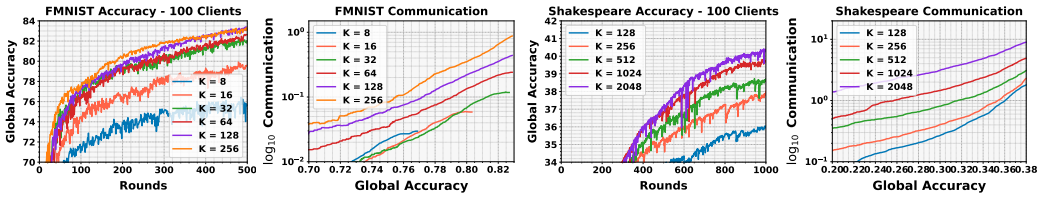

(a) FMNIST Accuracy (b) FMNIST Communication (c) Shakespeare Accuracy (d) Shakespeare Communication

Figure 6: Accuracy and communication cost per accuracy level for FMNIST and Shakespeare datasets. Demonstrating the effect of a number of trainable parameters (k) on the communication efficiency of MAPO.

consuming approximately 1% of the communication. Finally, in sequential tasks (Shakespeare and Sentiment140), MAPO retains up to 95.5% and 99.5% of FedAvg's accuracy, respectively, while dramatically reducing communication to less than 0.2%.

MAPO Hyperparameter. MAPO simplifies gradient projection by applying a single factorization across all model parameters, thus replacing per-layer rank selection with a single hyperparameter, k, directly controlling communication cost and model accuracy. Figure 6 illustrates the effect of varying k on performance and communication efficiency for the FMNIST and Shakespeare datasets. While a smaller k significantly reduces communication overhead, it slows the convergence, requiring more training rounds. Conversely, increasing k improves convergence speed and accuracy but rapidly raises communication costs, often with diminishing returns. Therefore, the optimal k achieves a target accuracy with minimal total communication. Figure 6(b) and (c) show communication costs associated with specific accuracy levels, guiding the selection of optimal k. We use the same guidelines for all baselines to fairly tune hyperparameters.

Fresh Reconstruction Matrix. A key factor in MAPO's performance is using a dynamically generated reconstruction matrix A rather than a fixed one. This approach promotes the exploration of new subspaces throughout training. Figure 7 illustrates the benefits of using a fresh A on the FMNIST and Shakespeare datasets. We evaluate MAPO across varying numbers of trainable parameters, ranging from 2^0 to 2^{13}. For FMNIST, this corresponds to 0.009% to 72.27% of the total model parameters, while for Shakespeare, it spans from 0.0001% to nearly 1%. In both cases, MAPO with a fresh A achieves superior convergence with fewer parameters, effectively leveraging the search space. In contrast, when A is frozen, performance follows a logarithmic correlation with the number of trainable parameters, requiring an exponentially larger parameter count to match the results obtained with a fresh A.

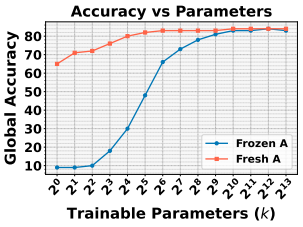

(A) FMNIST

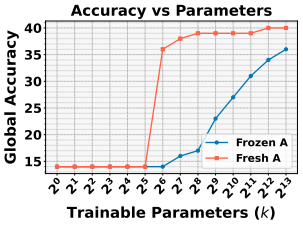

(B) Shakespeare

Figure 7: Comparison of having a fresh A vs. frozen A.

Additional Results. Comparisons with LoRA-based methods and Factorized-FL are provided in Appendices B and C. Appendix E supplements our main experiments with evaluations under IID distributions and without client sampling. Additionally, Appendix I presents a detailed memory complexity analysis, emphasizing MAPO's computational efficiency and flexibility compared to layer-wise low-rank factorization.

Limitations. MAPO's improved communication efficiency comes with additional computational overhead from gradient projection optimization. While significantly reduced compared to prior methods, MAPO still requires $\lceil d/r \rceil + r$ memory and computation (instead of $dr + r$; see Appendix I). MAPO complements, but does not replace, PEFT methods like LoRA, as it reduces communication overhead without decreasing the trainable parameters or storage requirements (see Appendix B).

7 Conclusion

We introduced *Model-Agnostic Projection Optimization* (MAPO), a novel approach for CEFL. Unlike layer-wise decomposition, MAPO factorizes the entire gradient using a projection vector and a random reconstruction matrix, regenerated at each round. MAPO balances communication efficiency and accuracy without imposing architecture-specific constraints or fixed-subspace limitations. Our theoretical analysis establishes convergence guarantees, and empirical results demonstrate superior performance and scalability across diverse datasets, confirming its practical value for FL.

References

[1] Brendan McMahan, Eider Moore, Daniel Ramage, Seth Hampson, and Blaise Aguera y Arcas. Communication-Efficient Learning of Deep Networks from Decentralized Data. In Aarti Singh and Jerry Zhu, editors, Proceedings of the 20th International Conference on Artificial Intelligence and Statistics, volume 54 of Proceedings of Machine Learning Research, pages 1273–1282. PMLR, 20–22 Apr 2017. URL https://proceedings.mlr.press/v54/mcmahan17a.html.

[2] Ninghui Jia, Zhihao Qu, Baoliu Ye, Yanyan Wang, Shihong Hu, and Song Guo. A comprehensive survey on communication-efficient federated learning in mobile edge environments. IEEE Communications Surveys & Tutorials, 2025.

[3] Jakub Konečnỳ. Federated learning: Strategies for improving communication efficiency. arXiv preprint arXiv:1610.05492, 2016.

[4] Tara N Sainath, Brian Kingsbury, Vikas Sindhwani, Ebru Arisoy, and Bhuvana Ramabhadran. Low-rank matrix factorization for deep neural network training with high-dimensional output targets. In 2013 IEEE international conference on acoustics, speech and signal processing, pages 6655–6659. IEEE, 2013.

[5] Edward J Hu, Yelong Shen, Phillip Wallis, Zeyuan Allen-Zhu, Yuanzhi Li, Shean Wang, Lu Wang, and Weizhu Chen. Lora: Low-rank adaptation of large language models. arXiv preprint arXiv:2106.09685, 2021.

[6] Yipeng Liu, Jiani Liu, Zhen Long, Ce Zhu, Yipeng Liu, Jiani Liu, Zhen Long, and Ce Zhu. Tensor decomposition in deep networks. Tensor Computation for Data Analysis, pages 241–263, 2022.

[7] Wenqi Wang, Yifan Sun, Brian Eriksson, Wenlin Wang, and Vaneet Aggarwal. Wide compression: Tensor ring nets. In Proceedings of the IEEE Conference on Computer Vision and Pattern Recognition, pages 9329–9338, 2018.

[8] Max Jaderberg, Andrea Vedaldi, and Andrew Zisserman. Speeding up convolutional neural networks with low rank expansions. arXiv preprint arXiv:1405.3866, 2014.

[9] Vadim Lebedev, Yaroslav Ganin, Maksim Rakhuba, Ivan Oseledets, and Victor Lempitsky. Speeding-up convolutional neural networks using fine-tuned cp-decomposition. arXiv preprint arXiv:1412.6553, 2014.

[10] Misha Denil, Babak Shakibi, Laurent Dinh, Marc'Aurelio Ranzato, and Nando De Freitas. Predicting parameters in deep learning. Advances in neural information processing systems, 26, 2013.

[11] Thijs Vogels, Sai Praneeth Karimireddy, and Martin Jaggi. Powersgd: Practical low-rank gradient compression for distributed optimization. In Advances in Neural Information Processing Systems (NeurIPS), volume 32, 2019.

[12] Jingfei Zhao, Ilia Shumailov, Takuma Chinen, Ilia Shumailov, and Dawn Song. Galore: Memory-efficient llm training by gradient low-rank projection. arXiv preprint arXiv:2306.03341, 2023.

[13] Haemin Park and Diego Klabjan. Communication-efficient federated low-rank update algorithm and its connection to implicit regularization. arXiv preprint arXiv:2409.12371, 2024.

[14] Mingzhao Guo, Dongzhu Liu, Osvaldo Simeone, and Dingzhu Wen. Low-rank gradient compression with error feedback for mimo wireless federated learning. arXiv preprint arXiv:2401.07496, 2024.

[15] Sixu Hu, Linshan Jiang, and Bingsheng He. Practical hybrid gradient compression for federated learning systems. In Proceedings of the Thirty-Third International Joint Conference on Artificial Intelligence, pages 4147–4155, 2024.

[16] D Yao, W Pan, Y Wan, H Jin, and L Sun. Fedhm: Efficient federated learning for heterogeneous models via low-rank factorization. arxiv. arXiv preprint arXiv:2111.14655, 2021.

[17] Nam Hyeon-Woo, Moon Ye-Bin, and Tae-Hyun Oh. Fedpara: Low-rank hadamard product for communication-efficient federated learning. arXiv preprint arXiv:2108.06098, 2021.

[18] Wonyong Jeong and Sung Ju Hwang. Factorized-fl: Personalized federated learning with parameter factorization & similarity matching. Advances in Neural Information Processing Systems, 35:35684–35695, 2022.

[19] Muhammad Ghufran Areeb Hameed, Thuong-Hai Bui, Yookyung Park, Shafiq Joty, and Steven CH Hoi. Rosa: Random subspace adaptation for efficient fine-tuning. In International Conference on Learning Representations (ICLR), 2023.

[20] Haoran Zhao, Jiayu Zhang, Qinbin Sun, Zhouchen Lin, Yang Wang, Yefeng Zheng, and Shiqiang Liu. Separate: A simple low-rank projection for gradient compression. arXiv preprint arXiv:2309.08386, 2023.

[21] Youbang Sun, Zitao Li, Yaliang Li, and Bolin Ding. Improving lora in privacy-preserving federated learning. arXiv preprint arXiv:2403.12313, 2024.

[22] Longteng Zhang, Lin Zhang, Shaohuai Shi, Xiaowen Chu, and Bo Li. Lora-fa: Memory-efficient low-rank adaptation for large language models fine-tuning. arXiv preprint arXiv:2308.03303, 2023.

[23] Jiacheng Zhu, Kristjan Greenewald, Kimia Nadjahi, Haitz Sáez de Ocáriz Borde, Rickard Brüel Gabrielsson, Leshem Choshen, Marzyeh Ghassemi, Mikhail Yurochkin, and Justin Solomon. Asymmetry in low-rank adapters of foundation models. arXiv preprint arXiv:2402.16842, 2024.

[24] Yongchang Hao, Yanshuai Cao, and Lili Mou. Flora: Low-rank adapters are secretly gradient compressors. arXiv preprint arXiv:2402.03293, 2024.

[25] Pengxin Guo, Shuang Zeng, Yanran Wang, Huijie Fan, Feifei Wang, and Liangqiong Qu. Selective aggregation for low-rank adaptation in federated learning. arXiv preprint arXiv:2410.01463, 2024.

[26] Mohammad Mahdi Rahimi, Hasnain Irshad Bhatti, Younghyun Park, Humaira Kousar, Do-Yeon Kim, and Jaekyun Moon. Evofed: leveraging evolutionary strategies for communication-efficient federated learning. Advances in Neural Information Processing Systems, 36, 2024.

[27] Dan Alistarh, Demjan Grubic, Jerry Li, Ryota Tomioka, and Milan Vojnovic. Qsgd: Communication-efficient sgd via gradient quantization and encoding. In Advances in Neural Information Processing Systems, pages 1709–1720, 2017.

[28] Yuzhu Mao, Zihao Zhao, Guangfeng Yan, Yang Liu, Tian Lan, Linqi Song, and Wenbo Ding. Communication-efficient federated learning with adaptive quantization. ACM Transactions on Intelligent Systems and Technology (TIST), 13(4):1–26, 2022.

[29] Jeremy Bernstein, Yu-Xiang Wang, Kamyar Azizzadenesheli, and Anima Anandkumar. signsgd: Compressed optimisation for non-convex problems. In International Conference on Machine Learning (ICML), 2018.

[30] Wei Wen, Cong Xu, Feng Yan, Chunpeng Wu, Yandan Wang, Yiran Chen, and Hai Li. Terngrad: Ternary gradients to reduce communication in distributed deep learning. In Advances in Neural Information Processing Systems (NeurIPS), volume 30, 2017.

[31] Yujun Lin, Song Han, Huizi Mao, Yu Wang, and William J Dally. Deep gradient compression: Reducing the communication bandwidth for distributed training. In International Conference on Learning Representations (ICLR), 2018.

[32] Amirhossein Reisizadeh, Aryan Mokhtari, Hamed Hassani, Ali Jadbabaie, and Ramtin Pedarsani. Fedpaq: A communication-efficient federated learning method with periodic averaging and quantization. In International Conference on Artificial Intelligence and Statistics, pages 2021–2031. PMLR, 2020.

[33] Shiqiang Sun, Jakub Konecny, Ananda Theertha Suresh, and Brendan McMahan. Qfedavg: Quantized federated averaging. arXiv preprint arXiv:2002.05645, 2020.

[34] Sheikh Shams Azam, Seyyedali Hosseinalipour, Qiang Qiu, and Christopher Brinton. Recycling model updates in federated learning: Are gradient subspaces low-rank? In International Conference on Learning Representations, 2021.

[35] Yongjeong Oh, Yo-Seb Jeon, Mingzhe Chen, and Walid Saad. Vector quantized compressed sensing for communication-efficient federated learning. In 2022 IEEE Globecom Workshops (GC Wkshps), pages 365–370. IEEE, 2022.

[36] Sangjun Park and Wan Choi. Regulated subspace projection based local model update compression for communication-efficient federated learning. IEEE Journal on Selected Areas in Communications, 41(4):964–976, 2023.

[37] Zai Shi and Atilla Eryilmaz. Communication-efficient subspace methods for high-dimensional federated learning. In 2021 17th International Conference on Mobility, Sensing and Networking (MSN), pages 543–550. IEEE, 2021.

[38] Gene H. Golub and Charles F. Van Loan. Matrix Computations. Johns Hopkins University Press, 3rd edition, 1996.

[39] David P. Woodruff. Sketching as a tool for numerical linear algebra. Foundations and Trends in Theoretical Computer Science, 10(1–2):1–157, 2014.

[40] Chunyuan Li, Hang Su, Xiaowei Shen, Yizhe Li, Yiren Wang, Yiming Chen, and Lawrence Carin. Measuring the intrinsic dimension of objective landscapes. In International Conference on Learning Representations (ICLR), 2018.

[41] Song Han, Huizi Mao, and William J Dally. Deep compression: Compressing deep neural networks with pruning, trained quantization and huffman coding. arXiv preprint arXiv:1510.00149, 2015.

[42] Yihui He, Xiangyu Zhang, and Jian Sun. Channel pruning for accelerating very deep neural networks. In Proceedings of the IEEE International Conference on Computer Vision (ICCV), 2017.

[43] Jian-Hao Luo, Jianxin Wu, and Weiyao Lin. Thinet: A filter level pruning method for deep neural network compression. In Proceedings of the IEEE international conference on computer vision, pages 5058–5066, 2017.

[44] Tianyun Zhang, Shaokai Ye, Kaiqi Zhang, Jian Tang, Wujie Wen, Makan Fardad, and Yanzhi Wang. A systematic dnn weight pruning framework using alternating direction method of multipliers. In Proceedings of the European conference on computer vision (ECCV), pages 184–199, 2018.

[45] Wenlin Chen, James Wilson, Stephen Tyree, Kilian Weinberger, and Yixin Chen. Compressing neural networks with the hashing trick. In International Conference on Machine Learning (ICML), 2015.

[46] Matthieu Courbariaux, Itay Hubara, Daniel Soudry, Ran El-Yaniv, and Yoshua Bengio. Binarized neural networks: Training deep neural networks with weights and activations constrained to +1 or -1. In Advances in Neural Information Processing Systems (NeurIPS), volume 29, 2016.

[47] Karen Ullrich, Edward Meeds, and Max Welling. Soft weight-sharing for neural network compression. arXiv preprint arXiv:1702.04008, 2017.

[48] Roman Vershynin. High-Dimensional Probability: An Introduction with Applications in Data Science. Cambridge Series in Statistical and Probabilistic Mathematics. Cambridge University Press, 1st edition, 2018.

[49] Terence Tao. Topics in Random Matrix Theory. Graduate Studies in Mathematics, Vol. 132. American Mathematical Society, 2012.

[50] Yann LeCun, Léon Bottou, Yoshua Bengio, and Patrick Haffner. Gradient-based learning applied to document recognition. Proceedings of the IEEE, 86(11):2278–2324, 1998.

[51] Han Xiao, Kashif Rasul, and Roland Vollgraf. Fashion-mnist: a novel image dataset for benchmarking machine learning algorithms. arXiv preprint arXiv:1708.07747, 2017.

[52] Alex Krizhevsky, Geoffrey Hinton, et al. Learning multiple layers of features from tiny images. Unpublished, 2009.

[53] Stanford University. Tiny imagenet visual recognition challenge. `https://www.kaggle.com/c/tiny-imagenet`, 2015.

[54] Sebastian Caldas, Sai Meher Karthik Duddu, Peter Wu, Tian Li, Jakub Konečnỳ, H Brendan McMahan, Virginia Smith, and Ameet Talwalkar. Leaf: A benchmark for federated settings. arXiv preprint arXiv:1812.01097, 2018.

[55] Alex Wang, Amanpreet Singh, Julian Michael, Felix Hill, Omer Levy, and Samuel R Bowman. Glue: A multi-task benchmark and analysis platform for natural language understanding. In Proceedings of the 2018 EMNLP Workshop BlackboxNLP: Analyzing and Interpreting Neural Networks for NLP, pages 353–355, 2018.

[56] James Bradbury, Roy Frostig, Peter Hawkins, Matthew James Johnson, Chris Leary, Dougal Maclaurin, George Necula, Adam Paszke, Jake VanderPlas, Skye Wanderman-Milne, and Qiao Zhang. JAX: composable transformations of Python+NumPy programs, 2018. URL `http://github.com/google/jax`.

[57] Yuexiang Xie, Zhen Wang, Dawei Gao, Daoyuan Chen, Liuyi Yao, Weirui Kuang, Yaliang Li, Bolin Ding, and Jingren Zhou. Federatedscope: A flexible federated learning platform for heterogeneity. Proceedings of the VLDB Endowment, 16(5):1059–1072, 2023.

A Accuracy and Communication Learning curves

This appendix provides extended experimental results that complement the main findings discussed in Section 5. We include detailed evaluations of MAPO and baseline methods on CIFAR-100, TinyImageNet, and Sentiment140 datasets. Similar to the main results, Figure 8 reports both maximum test accuracy and the communication cost required to reach a given accuracy threshold. These additional experiments further demonstrate MAPO's superior communication efficiency and consistent performance gains across more challenging and large-scale tasks.

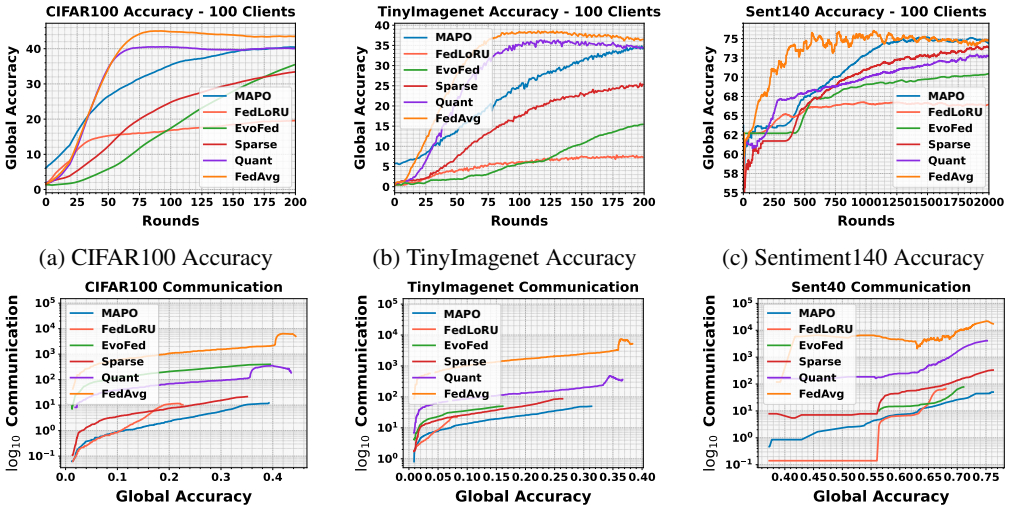

(a) CIFAR100 Accuracy (b) TinyImagenet Accuracy (c) Sentiment140 Accuracy

(d) CIFAR100 Comm. cost (e) TinyImagenet Comm. cost (f) Sentiment140 Comm. cost

Figure 8: **Performance comparison** of MAPO and baseline methods on CIFAR100, TinyImagenet, and Sentiment140 datasets. The top row shows the accuracy achieved by each method on the respective datasets, while the bottom row illustrates the communication cost associated with each method.

B Comparison with Low-Rank Adaptation in Fine-tuning

We conduct fine-tuning experiments using RoBERTa-large on five GLUE tasks to evaluate MAPO alongside LoRA, FA-LoRA, and SA-LoRA. Table 4 compares the number of trainable parameters and the communication load per round for each method. Table 5 summarizes fine-tuning results under federated settings, reporting communication efficiency based on the number of rounds and total communication required to reach 80% accuracy. Overall, the results indicate that MAPO improves communication efficiency without compromising performance.

Table 4: Number of trainable and communication parameters per round for different methods.

Method	Number of trainable parameters	Number of communication parameters per round
LoRA	1.83M	0.78M
FA-LoRA	1.44M	0.39M
SA-LoRA	1.83M	0.39M
MAPO$_{d/1k}$	357M	0.36M
MAPO$_{d/10k}$	357M	35.70K
MAPO$_{d/100k}$	357M	3.57K
MAPO$_{d/1m}$	357M	357

Table 5: Comparison of model accuracies, communication rounds, and total communication cost.

Model	SST2			QNLI			RTE			MNLIm			MNLImm		
	Acc	Round	Total	Acc	Round	Total	Acc	Round	Total	Acc	Round	Total	Acc	Round	Total
LoRA	84.86	36	28.08M	91.72	85	66.30M	86.62	180	140.40M	87.41	86	67.08M	87.34	82	63.96M
FA-LoRA	94.15	44	17.16M	91.63	76	29.64M	57.28	—	—	85.92	76	29.64M	86.46	213	83.07M
SA-LoRA	95.41	19	7.41M	91.04	55	21.45M	70.01	—	—	89.44	29	11.31M	85.49	126	49.14M
MAPO$_{d/1k}$	96.79	5	1.78M	93.14	11	3.93M	87.91	23	8.21M	88.90	17	6.07M	88.26	22	7.85M
MAPO$_{d/10k}$	96.10	5	178.50K	92.57	8	285.60K	89.57	23	821.10K	88.81	18	642.60K	87.43	25	892.50K
MAPO$_{d/100k}$	95.53	5	17.85K	89.24	7	24.99K	84.38	24	85.68K	85.04	20	71.40K	84.60	29	103.53K
MAPO$_{d/1m}$	90.37	7	2.50K	80.09	34	12.14K	57.04	—	—	72.46	—	—	37.76	—	—

C Comparison with Factorized-FL

In this section, we present a detailed comparison between MAPO and Factorized-FL as a representative of the parameter decomposition methods. Factorized-FL can be interpreted as a variant of rank-1 LoRA, where a sparse bias matrix substitutes for LoRA's frozen fine-tuned weights, initialized to zero. Table 6 reports the communication efficiency of MAPO and Factorized-FL on CIFAR-10 and SVHN datasets, evaluated under both IID and non-IID partitions. Each column denotes the total communication in GB required to reach X% of FedAvg's final test accuracy. Results show that MAPO achieves significantly lower communication costs compared to Factorized-FL while maintaining competitive performance across both datasets and data distributions.

Table 6: Communication cost comparison across different methods on SVHN and CIFAR-10 under IID and Non-IID settings.

Method	**SVHN**				**CIFAR-10**				**Com/Round**
	IID@80%	IID@90%	Non-IID@80%	Non-IID@90%	IID@80%	IID@90%	Non-IID@80%	Non-IID@90%	
FedAvg	183.51	244.68	285.46	509.75	305.85	407.80	326.24	652.48	20.39GB
Factorized-FL	127.75	182.50	146.00	219.00	182.50	292.00	200.75	310.25	18.25GB
MAPO_{2k}	0.32	0.79	0.56	–	0.32	–	0.94	–	**0.78MB**
MAPO_{16k}	**0.08**	**0.18**	**0.12**	**0.27**	**0.08**	**0.18**	**0.23**	**0.45**	6.25MB
MAPO_{40k}	3.84	8.64	5.76	13.12	3.84	8.64	10.88	21.12	0.32GB

D Implementation details and Hyperparameters

All experiments were conducted on a single NVIDIA RTX 3090 with 24 GB of memory. The main experiments and baselines are implemented with JAX [56]. The GLUE tasks and LLM fine-tuning implementation use Hugging Face libraries and models implemented in FederatedScope [57] with half precision (i.e., 16-bit float). The model configuration and training used in this work are provided in Tables 7 and 8.

Table 7: Neural network configurations for different datasets.

Dataset	**Model type**	**# Conv**	**Kernel**	**Hidden features**	**# Linear**	**# Output**	**# Parameters**
MNIST	CNN	2	5×5	8, 16	1	10	11.3K
FMNIST	CNN	2	5×5	8, 16	1	10	11.3K
CIFAR-10	CNN	4	5×5	64, 64, 128, 128	2	10	1.1M
CIFAR-100	WideResNet	16	3×3	64×4, 128×4	2	100	2.8M
TinyImageNet	WideResNet	16	3×3	64×4, 128×4	2	200	2.88M
Shakespeare	LSTM	-	-	256, 8 (embed)	2	65	814K
Sentiment140	Transformer	-	-	512, 96 (embed)	2	2	2.2M
SVHN	CNN	4	5×5	64, 64, 128, 128	2	10	1.1M
GLUE	RoBERTa-large	-	-	1024 (hidden)	2	Varies	357M

Table 8: Training hyperparameters for FedAvg and variants.

Hyperparameter	**MNIST**	**FMNIST**	**CIFAR-10**	**CIFAR-100**	**TinyImageNet**	**Sentiment140**	**Shakespeare**	**SVHN**	**GLUE**
Batch size	32	32	32	32	32	32	32	32	128
Optimizer	SGD	SGD	SGD	AdamW	AdamW	SGD	SGD	SGD	SGD
Learning rate	0.2	0.2	0.03	0.1	0.2	0.001	0.2	0.03	0.02
Momentum	0.9	0.9	0.4	0.9	0.9	0.9	0.9	0.4	0.0
L1 regularization	0.0	0.0	1e-4	0.0	1e-5	0.0	5e-6	1e-4	0.0
L2 regularization	0.0	0.0	1e-5	3e-3	1e-4	0.0	5e-5	1e-5	0.0

E IID and Client Sampling

This section includes the results of additional experiments on IID distribution and client sampling for MNIST, FMNIST, and CIFAR-10. Across all three datasets, we observe consistent trends. Reducing the fraction of clients participating (from all clients to 10%) moderately decreases accuracy for all methods, and non-IID settings introduce additional accuracy penalties. However, MAPO's performance remains robust in these more demanding scenarios; it routinely stays close to FedAvg's high-accuracy results while maintaining significant communication savings. This resilience suggests that MAPO's approach scales well to heterogeneous data distributions and partial-participation regimes, crucial in large-scale FL deployments.

Table 9: Extrapolated MNIST results for IID vs. non-IID and full vs. 10% client participation.

	IID				**Non-IID**			
	All clients		**10% clients**		**All clients**		**10% clients**	
Method	Com.	Acc.	Com.	Acc.	Com.	Acc.	Com.	Acc.
FedAvg	100%	99.6%	100%	99.5%	100%	99.3%	100%	98.9%
Sparse	10.0%	93.9%	12.0%	93.6%	13.3%	93.4%	15.3%	92.1%
Quantize	22.0%	98.8%	25.0%	98.5%	29.0%	98.2%	31.3%	97.6%
EvoFed	6.5%	99.4%	7.0%	99.2%	8.5%	**99.0%**	9.4%	**98.5%**
FedLoRU	22.0%	95.0%	25.0%	94.7%	28.2%	94.3%	30.2%	93.8%
MAPO	**2.0%**	**99.5%**	**2.3%**	**99.3%**	**2.7%**	**99.0%**	**2.9%**	**98.5%**

Table 10: Extrapolated FMNIST results for IID vs. non-IID and full vs. 10% client participation.

	IID				**Non-IID**			
	All clients		**10% clients**		**All clients**		**10% clients**	
Method	Com.	Acc.	Com.	Acc.	Com.	Acc.	Com.	Acc.
FedAvg	100%	91.5%	100%	91.0%	100%	90.0%	100%	89.2%
Sparse	16.0%	84.0%	19.0%	83.5%	21.0%	82.0%	24.1%	81.1%
Quantize	16.0%	89.7%	19.0%	89.2%	21.0%	88.0%	24.1%	87.1%
EvoFed	4.5%	87.0%	5.5%	86.5%	6.8%	85.5%	7.6%	84.7%
FedLoRU	12.0%	76.8%	14.0%	76.2%	15.5%	75.0%	17.9%	74.1%
MAPO	**2.0%**	**90.0%**	**2.3%**	**89.6%**	**2.7%**	**88.8%**	**3.1%**	**88.0%**

Table 11: Extrapolated CIFAR-10 results for IID vs. non-IID and full vs. 10% client participation.

	IID				**Non-IID**			
	All clients		**10% clients**		**All clients**		**10% clients**	
Method	Com.	Acc.	Com.	Acc.	Com.	Acc.	Com.	Acc.
FedAvg	100%	73.0%	100%	72.0%	100%	70.0%	100%	69.0%
Sparse	1.8%	41.0%	2.0%	40.0%	2.4%	38.0%	2.7%	37.2%
Quantize	10.0%	71.0%	12.0%	70.0%	13.0%	68.5%	15.2%	67.4%
EvoFed	2.0%	43.0%	2.5%	42.0%	3.0%	40.5%	3.4%	39.5%
FedLoRU	1.1%	27.0%	1.3%	26.0%	1.5%	24.5%	1.7%	23.5%
MAPO	**0.8%**	**71.5%**	**0.9%**	**70.8%**	**1.0%**	**69.2%**	**1.2%**	**68.3%**

F Notations

Table 12: Notation and Definitions

Symbol	Meaning / Definition
N	Number of layers in a model.
i	Indexing notation for the layers of the model. ($1 \leq i \leq N$)
M	Number of clients in FL.
j	Indexing notation for clients. ($1 \leq j \leq M$)
T	Total number of communication rounds in FL.
t	Indexing notation for rounds. ($1 \leq t \leq T$)
$\mathcal{D}^j$	Local dataset for client j.
b^j	Weight for client j, usually set as the number of local samples $\lvert\mathcal{D}^j\rvert$.
ΔW	Model update, treated as a single vector, $\in \mathbb{R}^{d\times 1}$.
W^t	Model parameters at communication round t.
$\overline{B}^t$	Aggregated projection vector at round t, broadcast by the server.
r^t	Random seed used to synchronize matrix generation across clients and the server.
A^t	Reconstruction matrix at round t, regenerated using r_t.
$B^{t,j}$	Trainable projection matrix for client j at round t.
$\hat{B}^{t,j}$	Locally optimized projection matrix for client j at round t.
η	Learning rate for local optimization.
d	Total number of model parameters, defined as $d = \sum_i d_1^i d_2^i$.
d_1^i, d_2^i	Row and column dimensions of the weight matrix for layer i.
p	Factorization rank after reshaping.
q	LoRA Factorization rank before reshaping.
k	Design parameter controlling reshape dimension ($\Delta W'$ reshaped into $\mathbb{R}^{\lceil d/k\rceil\times k}$).
$A \in \mathbb{R}^{\cdot\times\cdot}$, $B \in \mathbb{R}^{\cdot\times\cdot}$	Reconstruction and projection matrices in factorization.
$\mathcal{L}(W)$	Global loss function.
$\mathcal{L}^i(W)$	Local loss function for client i.
$\nabla\mathcal{L}(W)$	Gradient of the global loss function.
$\nabla B^{t,j}$	Gradient of local loss for the projection matrix.
σ_l^2	Bounded variance of stochastic gradients.
β	Smoothness constant of the loss function.
ϵ	Distortion parameter from the Johnson-Lindenstrauss Lemma.

G Proof of Definitions and Propositions

Definition G.1 (**Communication Overhead Rate**). Let $\Delta W \in \mathbb{R}^{d_1 \times d_2}$ be the update matrix of a model. Suppose the factorization of ΔW as $\Delta W = BA$, where $A \in \mathbb{R}^{q \times d_2}$ is a fixed random matrix and $B \in \mathbb{R}^{d_1 \times q}$ is a trainable matrix with $q \leq \min(d_1, d_2)$ being the factorization rank. The **communication overhead rate** CO_{rate} is defined as the ratio of the size of B to the size of ΔW:

$$\mathrm{CO}_{rate} = \frac{\mathrm{size}(B)}{\mathrm{size}(\Delta W)} = \frac{q}{d_2}.$$

Definition G.2 (**Reconstruction Error Rate**). Using the same factorization as Theorem 3.2, the *reconstruction error rate* is the expected ratio of the reconstruction error to the original model update. Given full-rank random reconstruction (Theorem 3.1), it is expressed as:

$$\frac{\mathbb{E}_A\left[\|\Delta W - BA\|_2^2\right]}{\|\Delta W\|_2^2} = 1 - \frac{q}{d_2}.$$

Proof. Let $\Delta W = [\Delta w_1 \ \Delta w_2 \ \cdots \ \Delta w_{d_1}]$, where each column $\Delta w_i \in \mathbb{R}^{d_2}$. Similarly, the reconstruction BA can be written as $[b_1 A \ b_2 A \ \cdots \ b_{d_1} A]$, where each $b_i \in \mathbb{R}^q$ is a trainable matrix. The reconstruction error is given by:

$$\|\Delta W - BA\|_2^2 = \sum_{i=1}^{d_1} \|\Delta w_i - b_i A\|_2^2.$$

The projection of Δw_i onto the subspace spanned by A is $P_A \Delta w_i$. The error rate E is defined as:

$$E = \frac{\|\Delta w_i - \Delta w_i P_A\|_2^2}{\|\Delta w_i\|_2^2}.$$

Using the Pythagorean theorem:

$$\|\Delta w_i\|_2^2 = \|\Delta w_i P_A\|_2^2 + \|w_i - \Delta w_i \ P_A|_2^2,$$

we rewrite E as:

$$E = \frac{\|\Delta w_i\|_2^2 - \|\Delta w_i P_A\|_2^2}{\|\Delta w_i\|_2^2} = 1 - \frac{\|\Delta w_i P_A\|_2^2}{\|\Delta w_i\|_2^2}.$$

The expected value of $\|\Delta w_i P_A\|_2^2$ for a full-rank random Gaussian projection is:

$$\mathbb{E}[\|\Delta w_i P_A\|_2^2] = \frac{q}{d_2} \|\Delta w_i\|_2^2.$$

Substituting this into E:

$$\mathbb{E}[\|\Delta w_i - b_i A\|_2^2] = 1 - \frac{\mathbb{E}[\|\Delta w_i P_A\|_2^2]}{\|\Delta w_i\|_2^2} = 1 - \frac{\frac{p}{d}\|\Delta w_i\|_2^2}{\|w_i\|_2^2} = 1 - \frac{q}{d_2}.$$

Applying this to each column $\Delta \Delta w_i$ of ΔW, we obtain:

$$\mathbb{E}_A\left[\sum_{i=1}^{d_1} \|\Delta w_i - b_i A\|_2^2\right] = \sum_{i=1}^{d_1} \mathbb{E}_A\left[\|\Delta w_i - (\Delta w_i) P_A\|_2^2\right].$$

Using the expected error formula:

$$= \sum_{i=1}^{d_1} \left(1 - \frac{q}{d_2}\right) \|\Delta w_i\|_2^2 = \left(1 - \frac{q}{d_2}\right) \sum_{i=1}^{d_1} \|\Delta w_i\|_2^2.$$

Since $\|\Delta W\|_2^2 = \sum_{i=1}^{d_1} \|\Delta w_i\|_2^2$, we get:

$$\mathbb{E}_A\left[\|\Delta W - BA\|_2^2\right] = \left(1 - \frac{q}{d_2}\right) \|\Delta W\|_2^2.$$

□

Proposition G.3 (**Single-Vector Factorization**). *Let ΔW, A, and B be factorizations of a single layer of the network as in Theorem 3.2. By reshaping ΔW into $\Delta W' \in \mathbb{R}^{1\times d_1 d_2}$ the factorization of $\Delta W' = B'A'$ where $A' \in \mathbb{R}^{p\times d_1 d_2}$ and $B' \in \mathbb{R}^{1\times p}$ can achieve the same **reconstruction error** and **communication overhead** to the conventional factorization of ΔW when $p = qd_1$.*

Proof of Error Preservation. In the single-vector setup, $\Delta W' \in \mathbb{R}^{d_1 d_2}$ is projected onto a subspace of dimension p. From random projection theory (as used in Theorem 3.3), if A' is sampled such that $\mathrm{rank}(A') = p$, then:

$$\mathbb{E}\left[\frac{\|\Delta W' - B'A'\|_2^2}{\|\Delta W'\|_2^2}\right] = 1 - \frac{p}{d_1 d_2}.$$

Substituting $p = qd_1$ gives:

$$1 - \frac{qd_1}{d_1 d_2} = 1 - \frac{q}{d_2}.$$

Hence, the expected reconstruction error satisfies:

$$\mathbb{E}\left[\|\Delta W' - B'A'\|_2^2\right] = \left(1 - \frac{q}{d_2}\right)\|\Delta W'\|_2^2,$$

which matches the original factorization. □

Proof of Communication Preservation. For $\Delta W' \in \mathbb{R}^{d_1 d_2}$, with the total size $\mathrm{size}(\Delta W') = d_1 d_2$, we have the communication overhead as:

$$\mathrm{size}(B') = p = qd_1.$$

Thus, the communication overhead is:

$$\mathrm{CO}'_{rate} = \frac{\mathrm{size}(B')}{\mathrm{size}(\Delta W')} = \frac{qd_1}{d_1 d_2} = \frac{q}{d_2},$$

which matches the original overhead.

Since both the expected reconstruction error and the communication overhead remain unchanged, the single-vector factorization with $p = qd_1$ is equivalent in terms of efficiency. □

Proposition G.4 (**Multi-Layer Factorization**). *Let ΔW_i, A_i, and B_i be **single-vector factorization** of i-th layer of the n-layered network as in Theorem 3.4. By concatenating the reshaped weights ΔW_i into $\Delta W' \in \mathbb{R}^{1\times d}$, where $d = \sum_{i=1}^{n} d_1^i d_2^i$. The factorization of $\Delta W' = B'A'$ where $A' \in \mathbb{R}^{p\times d}$ and $B' \in \mathbb{R}^{1\times p}$ can achieve the same **reconstruction error** and **communication overhead** to the single-vector factorization applied to each ΔW_i when $p = nq$.*

Proof of Error Preservation. For each layer i, a random full-rank matrix $A_i \in \mathbb{R}^{q\times d_2^i}$ yields an expected squared reconstruction error

$$\mathbb{E}\Big[\|\Delta W_i - B_i A_i\|_F^2\Big] \;=\; \Big(1 \;-\; \frac{q}{d_2^i}\Big)\|\Delta W_i\|_F^2.$$

Flattening ΔW_i into $\Delta W_i' \in \mathbb{R}^{(d_1^i d_2^i)\times 1}$, a single-vector projection of dimension $q\, d_1^i$ preserves this same error ratio (cf. Theorem 3.4).

When we concatenate all $\Delta W_i'$ into $\Delta W' \in \mathbb{R}^{1\times d}$, we form a block-structured vector. Let $p := n\, q$ and let $A' \in \mathbb{R}^{p\times d}$ be constructed from a Gaussian distribution. By the standard random-projection argument in dimension d with subspace size p,

$$\mathbb{E}\Big[\|\Delta W' - B'A'\|_2^2\Big] \;=\; \Big(1 \;-\; \frac{p}{d}\Big)\|\Delta W'\|_2^2.$$

Since $p = n\, q$, the overall ratio matches applying single-vector factorizations of rank q to each $\Delta W_i'$ individually. □

Proof of Communication Preservation. For each layer i, the single-vector factorization of ΔW_i introduces

$$\mathrm{size}(B_i) \;=\; q\, d_1^i, \quad \mathrm{size}(\Delta W_i) \;=\; d_1^i\, d_2^i, \quad \text{hence} \quad \frac{\mathrm{size}(B_i)}{\mathrm{size}(\Delta W_i)} \;=\; \frac{q}{d_1^i}.$$

Concatenating all $\Delta W_i'$ into $\Delta W' \in \mathbb{R}^{1\times d}$ gives $\text{size}(\Delta W') = d$, with

$$d \;=\; \sum_{i=1}^{n} d_1^i \, d_2^i.$$

Meanwhile, in the multi-layer factorization, the new trainable vector $B' \in \mathbb{R}^{1\times p}$ has

$$\text{size}(B') \;=\; p \;=\; n\,q.$$

Thus

$$\frac{\text{size}(B')}{\text{size}(\Delta W')} \;=\; \frac{n\,q}{\sum_{i=1}^{n}\big(d_1^i \, d_2^i\big)},$$

which matches the total overhead of n individual rank-q factorizations (one per layer) in aggregate. Consequently, the communication overhead rate is also preserved.

Since both the expected reconstruction error (per layer or in total) and the communication overhead remain the same, choosing $p = n\,q$ for $\Delta W'$ is equivalent to applying single-vector factorization of rank q separately to each layer. □

Proposition G.5 (MAPO Factorization). *Let ΔW, A, B, and rank p be a multi-layer factorization of a network as defined in Theorem 3.5. By reshaping $\Delta W \in \mathbb{R}^{1\times d}$ into $\Delta W' \in \mathbb{R}^{k\times\lceil d/k\rceil}$, and the factorization of $\Delta W' = B'A'$ where $A' \in \mathbb{R}^{1\times\lceil d/k\rceil}$ and $B' \in \mathbb{R}^{k\times 1}$, we can achieve the same **reconstruction error** and **communication overhead** to the multi-layer factorization of ΔW when $k = p$, while reducing the memory by a factor of k^2.*

Proof of Error Preservation. Since $\Delta W \in \mathbb{R}^{1\times d}$ is reshaped into $\Delta W' \in \mathbb{R}^{k\times\lceil d/k\rceil}$, we still have $\|\Delta W'\|_F^2 = \|\Delta W\|_2^2$. When $A' \in \mathbb{R}^{1\times\lceil d/k\rceil}$ is a suitable random projection (and $B' \in \mathbb{R}^{k\times 1}$ is fit accordingly), the rank-1 subspace of dimension 1 within $\lceil d/k\rceil$ induces the known expected error ratio

$$\mathbb{E}\Big[\|\Delta W' - B'A'\|_F^2\Big] \;=\; \big(1 - \tfrac{1}{\lceil d/k\rceil}\big)\,\|\Delta W'\|_F^2,$$

since the ambient dimension is $k \times \lceil d/k\rceil \;\approx d$. By taking $k = p$, we obtain (via standard random-projection arguments) the matching error ratio $1 - p/d$, up to negligible rounding. Therefore:

$$\mathbb{E}\Big[\|\Delta W' - B'A'\|_F^2\Big] \;=\; \big(1 - \frac{p}{d}\big)\,\|\Delta W'\|_F^2,$$

□

Proof of Communication Preservation. The matrix $B' \in \mathbb{R}^{k\times 1}$ has size k in total. Meanwhile, $\Delta W' \in \mathbb{R}^{k\times\lceil d/k\rceil}$ has size $k \times \lceil d/k\rceil \approx d$. Thus

$$\frac{\text{size}(B')}{\text{size}(\Delta W')} \;=\; \frac{k}{\lceil d/k\rceil\, k} \;\approx\; \frac{k}{d} = \frac{p}{d}.$$

Setting $k = p$ matches the original ratio $\frac{p}{d}$ from $B \in \mathbb{R}^{p\times 1}$ in the multi-layer factorization. □

Proof of Memory Reduction by Factor k^2. In standard rank-p factorizations for $\Delta W \in \mathbb{R}^{1\times d}$, one typically stores a $p \times d$ projection plus a $1 \times p$ vector, whose total size scales as $dp + p$. By contrast, $A' \in \mathbb{R}^{1\times\lceil d/k\rceil}$ plus $B' \in \mathbb{R}^{k\times 1}$ has combined size $\lceil d/k\rceil + k$. When $k = p$, the ratio of these sizes can be shown to drop by a factor of approximately k^2. Hence the approach allocates k^2 times less memory than a naive $p \times d$ plus $1 \times p$ arrangement. As $p = k$

$$\frac{dp + p}{\lceil d/k\rceil + k} = \frac{dk + k}{\lceil d/k\rceil + k} \approx \frac{d+1}{d/k^2 + 1} \approx k^2$$

Thus, the factorization $\Delta W' = B'A'$ with $k = p$ exactly preserves the original rank-p error and overhead while using k^2-fold less memory. □

H Proof of Theorem

H.1 Assumptions and Preliminaries

We restate the key assumptions required for the convergence analysis.

Assumption H.1. For each j, $\mathcal{L}^j(v)$ is β-smooth, i.e., $\left\|\nabla\mathcal{L}^j(u)-\nabla\mathcal{L}^j(v)\right\| \leq \beta\|u-v\|$ for any u, v.

Assumption H.2. Variance of the stochastic gradient of D^j is bounded for each client j, i.e.,

$$\mathbb{E}\Big[\Big\|\nabla\mathcal{L}^j(W) - \widetilde{\nabla}\mathcal{L}^j(W)\Big\|^2\Big] \leq \sigma_l^2$$

Lemma H.3 (Johnson-Lindenstrauss Lemma)**.** *Given $0 < \epsilon < 1$, a set of points $\{x_1, x_2, \ldots, x_M\} \subset \mathbb{R}^d$, and a target dimension $k = O\left(\frac{\log M}{\epsilon^2}\right)$, there exists a random linear mapping $P \in \mathbb{R}^{d\times k}$ such that for all i, j:*

$$(1-\epsilon)\|x_i - x_j\|^2 \leq \|x_iP - x_jP\|^2 \leq (1+\epsilon)\|x_i - x_j\|^2.$$

In our context, the random projection matrices $B^{t,j}$ and reconstruction matrices A^t satisfy the JL property with high probability.

H.2 Proof of Theorem 1

Theorem H.1. *Let the learning rate satisfy $\eta_t \leq \frac{1-4\epsilon}{4\beta(1+\epsilon)}$. Then, the algorithm achieves the bound:*

$$\frac{1}{4H_T}\sum_{t=0}^{T-1}\eta_t\mathbb{E}\left[\left\|\nabla\mathcal{L}(W^t)\right\|^2\right] \leq \frac{\mathbb{E}\left[\mathcal{L}(W^0)\right] - \mathcal{L}^*}{H^T} + 2(\epsilon+\beta+\beta\epsilon)\sigma_l^2\frac{1}{H^T}\sum_{t=0}^{T-1}\eta_t^2,$$

where $H_T = \sum_{t=0}^{T-1}\eta_t$, ϵ is JL Lemma distortion parameter, and $\mathcal{L}^*$ is the minimum value of $\mathcal{L}(W)$.

Proof. By the β-smoothness of $\mathcal{L}(W)$ and taking expectation on both sides, we have

$$\mathbb{E}\left[\mathcal{L}(W^{t+1}) - \mathcal{L}(W^t)\right] \leq \mathbb{E}\left[\left\langle\nabla\mathcal{L}(W^t), W^{t+1} - W^t\right\rangle\right] + \frac{\beta}{2}\mathbb{E}\left[\left\|W^{t+1} - W^t\right\|^2\right]. \tag{6}$$

Using the update rule $W^{t+1} = W^t - \eta_t\overline{B}_tA^t$, where $\overline{B}_t = \frac{1}{M}\sum_{j=1}^M B^{t,j}$, we can rewrite the first term as:

$$\begin{aligned}
\mathbb{E}\left[\left\langle\nabla\mathcal{L}(W^t), W^{t+1} - W^t\right\rangle\right] &= -\eta_t\mathbb{E}\left[\left\langle\nabla\mathcal{L}(W^t), \overline{B}^tA^t\right\rangle\right] \\
&= -\eta_t\mathbb{E}\left[\left\langle\nabla\mathcal{L}(W^t), \left(\frac{1}{M}\sum_{j=1}^M B^{t,j}\right)A^t\right\rangle\right] \\
&= -\eta_t\mathbb{E}\left[\left\langle\nabla\mathcal{L}(W^t), \frac{1}{M}\sum_{j=1}^M B^{t,j}A^t\right\rangle\right].
\end{aligned}$$

We decompose $B^{t,j}A^t$ as:

$$\widetilde{\nabla}\mathcal{L}^j(W^t) = B^{t,j}A^t + e^{t,j},$$

where $e^{t,j} = \widetilde{\nabla}\mathcal{L}^j(W^t) - B^{t,j}A^t$ is the projection error.

Substituting back, we have:

$$\mathbf{E} = \mathbb{E}\left[\left\langle\nabla\mathcal{L}(W^t), W^{t+1} - W^t\right\rangle\right] = -\eta_t\mathbb{E}\left[\left\langle\nabla\mathcal{L}(W^t), \frac{1}{M}\sum_{j=1}^M\left(\widetilde{\nabla}\mathcal{L}^j(W^t) - e^{t,j}\right)\right\rangle\right]$$

Separating it into A_1 and A_2:

$$\mathbf{E} = \underbrace{-\eta_t \mathbb{E}\left[\left\langle \nabla \mathcal{L}(W^t), \frac{1}{M}\sum_{j=1}^{M} \widetilde{\nabla}\mathcal{L}^j(W^t)\right\rangle\right]}_{A_1} + \underbrace{\eta_t \mathbb{E}\left[\left\langle \nabla \mathcal{L}(W^t), \frac{1}{M}\sum_{j=1}^{M} e^{t,j}\right\rangle\right]}_{A_2}.$$

We will now concentrate on A_1 as:

$$\begin{aligned}
A_1 &= -\eta_t \mathbb{E}\left[\left\langle \nabla \mathcal{L}(W^t), \frac{1}{M}\sum_{j=1}^{M} \nabla\mathcal{L}^j(W^t)\right\rangle\right] \\
&= -\frac{\eta_t}{M}\sum_{j=1}^{M} \mathbb{E}\left[\left\langle \nabla \mathcal{L}(W^t), \nabla\mathcal{L}^j(W^t)\right\rangle\right] \\
&\underset{(a)}{=} -\frac{\eta_t}{2M}\sum_{j=1}^{M}\left\{\mathbb{E}\left[\|\nabla \mathcal{L}(W^t)\|^2\right] + \mathbb{E}\left[\left\|\nabla\mathcal{L}^j(W^t)\right\|^2\right]\right\} \\
&\quad + \frac{\eta_t}{2}\mathbb{E}\left[\left\| \underbrace{\nabla \mathcal{L}(W^t) - \frac{1}{M}\sum_{j=1}^{M}\nabla\mathcal{L}^j(W^t)}_{=0}\right\|^2\right] \\
&= -\frac{\eta_t}{2}\mathbb{E}\left[\|\nabla \mathcal{L}(W^t)\|^2\right] - \frac{\eta_t}{2M}\sum_{j=1}^{M}\mathbb{E}\left[\left\|\nabla\mathcal{L}^j(W^t)\right\|^2\right]
\end{aligned}$$

where (a) uses $\langle a, b\rangle = \frac{1}{2}\{||a||^2 + ||b||^2 - ||a-b||^2\}$. We now turn our attention to A_2 as:

Next, we focus on A_2:

$$\begin{aligned}
A_2 &= \eta_t \mathbb{E}\left[\left\langle \nabla \mathcal{L}(W^t), \frac{1}{M}\sum_{j=1}^{M} e^{t,j}\right\rangle\right] \\
&\underset{(a)}{\leq} \frac{\eta_t}{4}\mathbb{E}\left[\left\|\nabla \mathcal{L}(W^t)\right\|^2\right] + \eta_t \mathbb{E}\left[\left\|\frac{1}{M}\sum_{j=1}^{M} e^{t,j}\right\|^2\right] \\
&\underset{(b)}{\leq} \frac{\eta_t}{4}\mathbb{E}\left[\left\|\nabla \mathcal{L}(W^t)\right\|^2\right] + \frac{\eta_t}{M}\mathbb{E}\left[\left\|\sum_{j=1}^{M} e^{t,j}\right\|^2\right] \\
&\underset{(c)}{\leq} \frac{\eta_t}{4}\mathbb{E}\left[\left\|\nabla \mathcal{L}(W^t)\right\|^2\right] + \frac{\epsilon\eta_t}{M}\mathbb{E}\left[\left\|\sum_{j=1}^{M} \widetilde{\nabla}\mathcal{L}^j(W^t)\right\|^2\right] \\
&\underset{(d)}{\leq} \frac{\eta_t}{4}\mathbb{E}\left[\left\|\nabla \mathcal{L}(W^t)\right\|^2\right] + \frac{2\epsilon\eta_t}{M}\sum_{j=1}^{M}\left\{\mathbb{E}\left[\left\|\nabla\mathcal{L}^j(W^t)\right\|^2\right] + \mathbb{E}\left[\left\|\widetilde{\nabla} L_i(W^t) - \nabla\mathcal{L}^j(W^t)\right\|^2\right]\right\} \\
&\underset{(e)}{\leq} \frac{\eta_t}{4}\mathbb{E}\left[\left\|\nabla \mathcal{L}(W^t)\right\|^2\right] + \frac{2\epsilon\eta_t}{M}\sum_{j=1}^{M}\mathbb{E}\left[\left\|\nabla\mathcal{L}^j(W^t)\right\|^2\right] + 2\epsilon\eta_t^2\sigma_l^2
\end{aligned}$$

where (a) uses $\langle a, b\rangle \leq \frac{1}{4}\|a\|^2 + \|b\|^2$, and (b) follows Jensen's inequality, (c) comes from JL Lemma, (d) follows the inequality $\|a+b\|^2 \leq 2\|a\|^2 + 2\|b\|^2$, and (e) is based on Assumption 2. On the other hand, we can also place a bound on the second term $\mathbb{E}\left[\|W^{t+1} - W^t\|^2\right]$ as shown below:

$$
\begin{aligned}
\mathbb{E}\left[\|W^{t+1} - W^t\|^2\right] &= \mathbb{E}\left[\left\|\eta_t \overline{B_t} A^t\right\|^2\right] = \mathbb{E}\left[\left\|\eta_t \left(\frac{1}{M}\sum_{j=1}^{M} B^{t,j}\right) A^t\right\|^2\right] \\
&\underset{(a)}{\leq} 2\eta_t^2 \mathbb{E}\left[\left\|\frac{1}{M}\sum_{j=1}^{M} \widetilde{\nabla}\mathcal{L}^j(W^t)\right\|^2\right] + 2\eta_t^2 \mathbb{E}\left[\left\|\frac{1}{M}\sum_{j=1}^{M}\left\{B^{t,j}A^t - \widetilde{\nabla}\mathcal{L}^j(W^t)\right\}\right\|^2\right] \\
&\underset{(b)}{\leq} \frac{2\eta_t^2}{M} \mathbb{E}\left[\left\|\sum_{j=1}^{M} \widetilde{\nabla}\mathcal{L}^j(W^t)\right\|^2\right] + \frac{2\eta_t^2}{M} \mathbb{E}\left[\left\|\sum_{j=1}^{M}\left\{B^{t,j}A^t - \widetilde{\nabla}\mathcal{L}^j(W^t)\right\}\right\|^2\right] \\
&= \frac{2\eta_t^2}{M} \mathbb{E}\left[\left\|\sum_{j=1}^{M} \widetilde{\nabla}\mathcal{L}^j(W^t)\right\|^2\right] + \frac{2\eta_t^2}{M} \mathbb{E}\left[\left\|\sum_{j=1}^{M} e^{t,j}\right\|^2\right] \\
&\underset{(c)}{\leq} \frac{4\eta_t^2}{M}\sum_{j=1}^{M}\left\{\mathbb{E}\left[\left\|\nabla\mathcal{L}^j(W^t)\right\|^2\right] + \mathbb{E}\left[\left\|\widetilde{\nabla}L_i(W^t) - \nabla\mathcal{L}^j(W^t)\right\|^2\right]\right\} + \frac{2\eta_t^2}{M}\mathbb{E}\left[\left\|\sum_{j=1}^{M} e^{t,j}\right\|^2\right] \\
&\underset{(d)}{\leq} \frac{4\eta_t^2}{M}\sum_{j=1}^{M}\mathbb{E}\left[\left\|\nabla\mathcal{L}^j(W^t)\right\|^2\right] + \frac{2\eta_t^2}{M}\mathbb{E}\left[\left\|\sum_{j=1}^{M} e^{t,j}\right\|^2\right] + 4\eta_t^2\sigma_l^2 \\
&\underset{(e)}{\leq} \frac{4\eta_t^2}{M}\sum_{j=1}^{M}\mathbb{E}\left[\left\|\nabla\mathcal{L}^j(W^t)\right\|^2\right] + \frac{2\epsilon\eta_t^2}{M}\mathbb{E}\left[\left\|\sum_{j=1}^{M} \widetilde{\nabla}\mathcal{L}^j(W^t)\right\|^2\right] + 4\eta_t^2\sigma_l^2 \\
&\underset{(f)}{\leq} \frac{4\eta_t^2}{M}\sum_{j=1}^{M}\mathbb{E}\left[\left\|\nabla\mathcal{L}^j(W^t)\right\|^2\right] \\
&+ \frac{4\epsilon\eta_t^2}{M}\sum_{j=1}^{M}\left\{\mathbb{E}\left[\left\|\nabla\mathcal{L}^j(W^t)\right\|^2\right] + \mathbb{E}\left[\left\|\widetilde{\nabla}\mathcal{L}^j(W^t) - \nabla\mathcal{L}^j(W^t)\right\|^2\right]\right\} + 4\eta_t^2\sigma_l^2 \\
&\underset{(g)}{\leq} \frac{4\eta_t^2}{M}\sum_{j=1}^{M}\mathbb{E}\left[\left\|\nabla\mathcal{L}^j(W^t)\right\|^2\right] + \frac{4\epsilon\eta_t^2}{M}\sum_{j=1}^{M}\mathbb{E}\left[\left\|\nabla\mathcal{L}^j(W^t)\right\|^2\right] + 4\epsilon\eta_t^2\sigma_l^2 + 4\eta_t^2\sigma_l^2 \\
&= \frac{4(1+\epsilon)\eta_t^2}{M}\sum_{j=1}^{M}\mathbb{E}\left[\left\|\nabla\mathcal{L}^j(W^t)\right\|^2\right] + 4(1+\epsilon)\eta_t^2\sigma_l^2
\end{aligned}
$$

where (a), (c), and (f) are based on the inequality $\|a+b\|^2 \leq 2\|a\|^2 + 2\|b\|^2$, (b) comes from Jensen's inequality, (d), (g) derive from Assumption 2, and (e) comes from JL Lemma.

By utilizing the established bounds for $\mathbb{E}\left[\langle \nabla \mathcal{L}(W^t), W^{t+1} - W^t \rangle\right]$ and $\mathbb{E}\left[\|W^{t+1} - W^t\|^2\right]$ to Equation (6), we derive the following:

$$
\begin{aligned}
&\mathbb{E}\left[\mathcal{L}(W^{t+1}) - \mathcal{L}(W^t)\right] \leq \mathbb{E}\left[\langle \nabla \mathcal{L}(W^t), W^{t+1} - W^t \rangle\right] + \frac{\beta}{2}\mathbb{E}\left[\|W^{t+1} - W^t\|^2\right] \\
&\leq \underbrace{-\frac{\eta_t}{2}\mathbb{E}\left[\|\nabla \mathcal{L}(W^t)\|^2\right] - \frac{\eta_t}{2M}\sum_{j=1}^{M}\mathbb{E}\left[\left\|\nabla \mathcal{L}^j(W^t)\right\|^2\right]}_{A_1} \\
&\underbrace{+ \frac{\eta_t}{4}\mathbb{E}\left[\left\|\nabla \mathcal{L}(W^t)\right\|^2\right] + \frac{2\epsilon\eta_t}{M}\sum_{j=1}^{M}\mathbb{E}\left[\left\|\nabla \mathcal{L}^j(W^t)\right\|^2\right] + 2\epsilon\eta_t^2\sigma_l^2}_{A_2} \\
&+ \frac{2\beta(1+\epsilon)\eta_t^2}{M}\sum_{j=1}^{M}\mathbb{E}\left[\left\|\nabla \mathcal{L}^j(W^t)\right\|^2\right] + 2\beta(1+\epsilon)\eta_t^2\sigma_l^2 \\
&= -\frac{\eta_t}{4}\mathbb{E}\left[\|\nabla \mathcal{L}(W^t)\|^2\right] \\
&+ \frac{\eta_t}{M}\underbrace{\left\{-\frac{1}{2} + 2\epsilon + 2\beta(1+\epsilon)\eta_t\right\}}_{\leq 0 \text{ if we choose } \eta_t \leq \frac{1-4\epsilon}{4\beta(1+\epsilon)}}\sum_{j=1}^{M}\mathbb{E}\left[\left\|\nabla \mathcal{L}^j(W^t)\right\|^2\right] + 2\eta_t^2(\epsilon + \beta + \beta\epsilon)\sigma_l^2 \\
&\leq -\frac{\eta_t}{4}\mathbb{E}\left[\|\nabla \mathcal{L}(W^t)\|^2\right] + 2\eta_t^2(\epsilon + \beta + \beta\epsilon)\sigma_l^2
\end{aligned}
$$

Ultimately, by applying the telescoping sum over $t = 0, 1, \ldots, T-1$, we arrive at the following result:

$$
\mathcal{L}^* - \mathbb{E}\left[\mathcal{L}(W^0)\right] \leq \sum_{t=0}^{T-1} -\frac{\eta_t}{4}\mathbb{E}\left[\left\|\nabla \mathcal{L}(W^t)\right\|^2\right] + \sum_{t=0}^{T-1} 2\eta_t^2(\epsilon + \beta + \beta\epsilon)\sigma_l^2
$$

In this case, $\mathcal{L}^*$ stands for the minimum of $\mathcal{L}(W)$.

By performing a division by $H_T = \sum_{t=0}^{T-1}\eta_t$ on both sides and utilizing some algebraic adjustments, we arrive at the following expression:

$$
\frac{1}{4H_T}\sum_{t=0}^{T-1}\eta_t\mathbb{E}\left[\left\|\nabla \mathcal{L}(W^t)\right\|^2\right] \leq \frac{\mathbb{E}\left[\mathcal{L}(W^0)\right] - \mathcal{L}^*}{H_T} + 2(\epsilon + \beta + \beta\epsilon)\sigma_l^2\left(\frac{1}{H_T}\sum_{t=0}^{T-1}\eta_t^2\right) \tag{7}
$$

With a decreasing learning rate such as $\eta_t = \frac{\eta_0}{t+1}$, we observe that $H_T = \sum_{t=0}^{T-1}\eta_t$ tends towards infinity as T grows, while $\sum_{t=0}^{T-1}\eta_t^2$ remains bounded. Therefore, as $T \to \infty$, the upper bound in Equation (7) converges to 0, confirming the convergence to a stationary point. □

I Complexity Analysis and MAPO Flexibility

Theorems 3.4 to 3.6 discussed how the error rate and accuracy of low-rank factorization are only determined by the size of the projection vector regardless of reshaping and vectorization of layers. Although they prove that MAPO can achieve the same performance as layer-wise factorization given the same projection (communication) budget, we did not discuss the memory and computation complexity. In this section, we show that MAPO can effectively reduce computation. Furthermore, we show how layer-wise low-rank adaptation (LoRA and FA-LoRA) limits the model trade-offs and how MAPO can offer more flexibility.

I.1 Computational Complexity

We compute the memory and computation cost for matrix allocation and multiplication in terms of standard matrix multiplication. Given matrices $A \in \mathbb{R}^{n\times m}$ and $B \in \mathbb{R}^{p\times n}$, the complexities for computing $C = BA$ are:

$$\text{Memory}_{C=AB} = O(nm + pn + pm),$$

$$\text{Time}_{C=BA} = O(mnp).$$

We aim to demonstrate that factorization under MAPO, where $W \in \mathbb{R}^{k\times\lceil\frac{d}{k}\rceil}$ is factorized into $A \in \mathbb{R}^{1\times\lceil\frac{d}{k}\rceil}$ and $B \in \mathbb{R}^{k\times 1}$, reduces the memory and time complexity of the LoRA factorization for an n-layered model. In LoRA, each layer i is factorized as $w_i \in \mathbb{R}^{d_i^1\times d_i^2}$ into $A \in \mathbb{R}^{q\times d_i^1}$ and $B \in \mathbb{R}^{d_i^2\times q}$.

We demonstrate that, given the same communication budget and factorization error rate, MAPO significantly reduces the computational cost compared to LoRA. This reduction becomes more pronounced as the number of layers or the selected rank increases. Specifically, MAPO achieves a **memory reduction** by a factor of q^2 and a **computation reduction** by a factor of q, where q is the chosen LoRA rank. Furthermore, even when $q = 1$, MAPO still achieves memory savings as $\sum_{i\neq j}^{n} d_i^1 d_i^2$ scales with the number of layers. The only scenario where MAPO and LoRA yield identical efficiency is when the model consists of a single layer ($n = 1$) and a rank-1 factorization ($q = 1$).

Memory Complexity

Given these definitions, the memory complexities for MAPO and LoRA are:

$$\text{Memory}_{MAPO} = O\left(\left\lceil\frac{d}{k}\right\rceil + k + \left\lceil\frac{d}{k}\right\rceil k\right) \approx O\left(\frac{d}{k} + k + d\right),$$

$$\text{Memory}_{LoRA} = O\left(\sum_{i=1}^{n}(d_i^1 q + d_i^2 q + d_i^1 d_i^2)\right) = O\left(\sum_{i=1}^{n} d_i^1 q + \sum_{i=1}^{n} d_i^2 q + \sum_{i=1}^{n} d_i^1 d_i^2\right).$$

Given the same communication budget $k = \sum_{i=1}^{n} q d_i^1$ and $d = \sum_{i=1}^{n} d_i^1 d_i^2$, we rewrite LoRA's memory complexity as:

$$\text{Memory}_{LoRA} = O\left(q\sum_{i=1}^{n} d_i^2 + k + d\right).$$

For MAPO to have lower memory usage than LoRA, the following condition must hold:

$$\text{Memory}_{MAPO} \leq \text{Memory}_{LoRA},$$

$$\frac{d}{k} + k + d \leq q\sum_{i=1}^{n} d_i^2 + k + d,$$

$$\frac{d}{k} \leq q\sum_{i=1}^{n} d_i^2.$$

Replacing k and d with their respective summation terms:

$$\sum_{i=1}^{n} d_i^1 d_i^2 \leq q^2 \sum_{i=1}^{n} d_i^1 \sum_{i=1}^{n} d_i^2,$$
$$\leq q^2 \sum_{i=1}^{n} d_i^1 d_i^2 + q^2 \sum_{i \neq j}^{n} d_i^1 d_i^2.$$

Thus, the inequality always holds under the conditions $d_i^1, d_i^2, q, n \geq 1$, and equality occurs if $q = n = 1$, which corresponds to a model with a single layer and rank-1 factorization. In this case, MAPO and LoRA perform the same decomposition.

Time Complexity

Given the definitions, we can express the time complexities for MAPO and LoRA as follows:

$$\text{Time}_{MAPO} = O\left(\left\lceil \frac{d}{k} \right\rceil k\right) \approx O(d),$$
$$\text{Time}_{LoRA} = O\left(\sum_{i=1}^{n} q d_i^1 d_i^2\right).$$

Since $d = \sum_{i=1}^{n} d_i^1 d_i^2$, we can rewrite LoRA's time complexity as:

$$\text{Time}_{LoRA} = O(qd).$$

For MAPO to have a lower time complexity than LoRA, the following condition must hold:

$$\text{Time}_{MAPO} \leq \text{Time}_{LoRA},$$
$$d \leq qd.$$

This condition is always true for $d, q \geq 1$, and equality occurs when $q = 1$.

I.2 MAPO Flexibility

Suppose our neural network has n layers. Let:

$$W_i \in \mathbb{R}^{d_i^1 \times d_i^2} \quad \text{for each layer } i = 1, \ldots, n.$$

Let $d = \sum_{i=1}^{n} d_i^1 d_i^2$ be the total number of parameters (i.e., the sum of the entries across all layers). Let

$$d_1 \;=\; \sum_{i=1}^{n} d_i^1.$$

In many treatments of LoRA, the main communication or factor-size bottleneck arises from a factor that scales linearly with $q \cdot d_i^1$.

LoRA Factorization Per Layer. LoRA factorizes each layer W_i of dimension $d_i^1 \times d_i^2$ with a fixed rank q. Concretely,

$$W_i \;\approx\; W_i + B_i A_i, \qquad A_i \in \mathbb{R}^{q \times d_i^2}, \quad B_i \in \mathbb{R}^{d_i^1 \times q}.$$

The number of additional parameters introduced by each low-rank pair (A_i, B_i) is

$$\underbrace{d_i^1 \cdot q}_{\text{size of } B_i} \;+\; \underbrace{q \cdot d_i^2}_{\text{size of } A_i} \;=\; q\,(d_i^1 + d_i^2).$$

Summing over all n layers,

$$\sum_{i=1}^{n} \big(d_i^1 \cdot q + q \cdot d_i^2\big) \;=\; q \sum_{i=1}^{n} \big(d_i^1 + d_i^2\big).$$

Therefore, we can write the communication cost as:

$$\text{Communication cost} \;\approx\; q \sum_{i=1}^{n} d_i^1 \;=\; q\, d_1.$$

Since q must be an integer, we see that the communication overhead comes in integer multiplesd_1, as:

$$\text{LoRA total communication} \;\in\; \{\, q\, d_1 \;\mid\; q = 1, 2, \ldots \}.$$

There is no way to select a non-integer q. Hence communication budgets strictly between d_1 and $2\, d_1$ (or between $q\, d_1$ and $(q+1)d_1$) are not possible in layer-wise LoRA. Therefore, Any attempt to finely tune the communication or factor budget (e.g., to $1.5\, d_1$) is disallowed by LoRA's integral-rank requirement. This **rigidity** is precisely what we seek to overcome in MAPO.

MAPO Factorization. MAPO flattens or reshapes all parameters into one large matrix and then performs a single low-rank factorization with rank 1. A simplified abstraction is:

1. Reshape $w_1, \ldots, w_n$ into a single matrix $W \in \mathbb{R}^{k \times \lceil d/k \rceil}$, where $d = \sum_{i=1}^{n} d_i^1\, d_i^2$ is the total parameter count. 2. Factor $W \approx A\, B$, with

$$A \in \mathbb{R}^{1 \times \lceil d/k \rceil}, \quad B \in \mathbb{R}^{k \times 1},$$

Once all parameters are merged, MAPO can proportionally allocate any communication budget as k can be selected freely.

$$\underbrace{\lceil d/k \rceil}_{\text{size of } A} \;+\; \underbrace{k}_{\text{size of } B}.$$

Therefore, we can write the total communication as:

$$\text{MAPO total communication} \;\in\; \{\, k \;\mid\; k = 1, 2, \ldots \}.$$

This is particularly important in communication-efficient FL since viable solutions can be found with communication cost $k < d_1$ or $d_1 < k < 2d_1$, which architecture-dependent layer-wise factorization can not offer.

NeurIPS Paper Checklist

1. **Claims**

   Question: Do the main claims made in the abstract and introduction accurately reflect the paper's contributions and scope?

   Answer: [Yes]

   Justification: The Abstract and Introduction (§1) enumerate MAPO's three contributions, model-wide factorization, flexible communication, and convergence theory, which are exactly the results proven in §3–4 and confirmed experimentally in §5.

   Guidelines:

   - The answer NA means that the abstract and introduction do not include the claims made in the paper.
   - The abstract and/or introduction should clearly state the claims made, including the contributions made in the paper and important assumptions and limitations. A No or NA answer to this question will not be perceived well by the reviewers.
   - The claims made should match theoretical and experimental results, and reflect how much the results can be expected to generalize to other settings.
   - It is fine to include aspirational goals as motivation as long as it is clear that these goals are not attained by the paper.

2. **Limitations**

   Question: Does the paper discuss the limitations of the work performed by the authors?

   Answer: [Yes]

   Justification: §"Limitations" at the end of §6 (p. 9) and Appendix I openly note MAPO's extra per-round compute, memory trade-offs, and its complementarity, rather than replacement of PEFT methods.

   Guidelines:

   - The answer NA means that the paper has no limitation while the answer No means that the paper has limitations, but those are not discussed in the paper.
   - The authors are encouraged to create a separate "Limitations" section in their paper.
   - The paper should point out any strong assumptions and how robust the results are to violations of these assumptions (e.g., independence assumptions, noiseless settings, model well-specification, asymptotic approximations only holding locally). The authors should reflect on how these assumptions might be violated in practice and what the implications would be.
   - The authors should reflect on the scope of the claims made, e.g., if the approach was only tested on a few datasets or with a few runs. In general, empirical results often depend on implicit assumptions, which should be articulated.
   - The authors should reflect on the factors that influence the performance of the approach. For example, a facial recognition algorithm may perform poorly when image resolution is low or images are taken in low lighting. Or a speech-to-text system might not be used reliably to provide closed captions for online lectures because it fails to handle technical jargon.
   - The authors should discuss the computational efficiency of the proposed algorithms and how they scale with dataset size.
   - If applicable, the authors should discuss possible limitations of their approach to address problems of privacy and fairness.
   - While the authors might fear that complete honesty about limitations might be used by reviewers as grounds for rejection, a worse outcome might be that reviewers discover limitations that aren't acknowledged in the paper. The authors should use their best judgment and recognize that individual actions in favor of transparency play an important role in developing norms that preserve the integrity of the community. Reviewers will be specifically instructed to not penalize honesty concerning limitations.

3. **Theory assumptions and proofs**

   Question: For each theoretical result, does the paper provide the full set of assumptions and a complete (and correct) proof?

   Answer: [Yes]

   Justification: All assumptions are stated at the start of §4; full proofs for Propositions 1–3 and Theorem 1 are given in Appendix G–H.

   Guidelines:

   - The answer NA means that the paper does not include theoretical results.
   - All the theorems, formulas, and proofs in the paper should be numbered and cross-referenced.
   - All assumptions should be clearly stated or referenced in the statement of any theorems.
   - The proofs can either appear in the main paper or the supplemental material, but if they appear in the supplemental material, the authors are encouraged to provide a short proof sketch to provide intuition.
   - Inversely, any informal proof provided in the core of the paper should be complemented by formal proofs provided in appendix or supplemental material.
   - Theorems and Lemmas that the proof relies upon should be properly referenced.

4. **Experimental result reproducibility**

   Question: Does the paper fully disclose all the information needed to reproduce the main experimental results of the paper to the extent that it affects the main claims and/or conclusions of the paper (regardless of whether the code and data are provided or not)?

   Answer: [Yes]

   Justification: Dataset splits, non-IID partition rules, model specs, and every training hyperparameter are in Tables 2, 7, 8 (Appendix D); All codes and scripts are included in the anonymous supplementary zip.

   Guidelines:

   - The answer NA means that the paper does not include experiments.
   - If the paper includes experiments, a No answer to this question will not be perceived well by the reviewers: Making the paper reproducible is important, regardless of whether the code and data are provided or not.
   - If the contribution is a dataset and/or model, the authors should describe the steps taken to make their results reproducible or verifiable.
   - Depending on the contribution, reproducibility can be accomplished in various ways. For example, if the contribution is a novel architecture, describing the architecture fully might suffice, or if the contribution is a specific model and empirical evaluation, it may be necessary to either make it possible for others to replicate the model with the same dataset, or provide access to the model. In general. releasing code and data is often one good way to accomplish this, but reproducibility can also be provided via detailed instructions for how to replicate the results, access to a hosted model (e.g., in the case of a large language model), releasing of a model checkpoint, or other means that are appropriate to the research performed.
   - While NeurIPS does not require releasing code, the conference does require all submissions to provide some reasonable avenue for reproducibility, which may depend on the nature of the contribution. For example
     (a) If the contribution is primarily a new algorithm, the paper should make it clear how to reproduce that algorithm.
     (b) If the contribution is primarily a new model architecture, the paper should describe the architecture clearly and fully.
     (c) If the contribution is a new model (e.g., a large language model), then there should either be a way to access this model for reproducing the results or a way to reproduce the model (e.g., with an open-source dataset or instructions for how to construct the dataset).

(d) We recognize that reproducibility may be tricky in some cases, in which case authors are welcome to describe the particular way they provide for reproducibility. In the case of closed-source models, it may be that access to the model is limited in some way (e.g., to registered users), but it should be possible for other researchers to have some path to reproducing or verifying the results.

5. **Open access to data and code**

   Question: Does the paper provide open access to the data and code, with sufficient instructions to faithfully reproduce the main experimental results, as described in supplemental material?

   Answer: [Yes]

   Justification: The supplementary material contains the code and scripts; all datasets are publicly available.

   Guidelines:

   - The answer NA means that paper does not include experiments requiring code.
   - Please see the NeurIPS code and data submission guidelines (`https://nips.cc/public/guides/CodeSubmissionPolicy`) for more details.
   - While we encourage the release of code and data, we understand that this might not be possible, so "No" is an acceptable answer. Papers cannot be rejected simply for not including code, unless this is central to the contribution (e.g., for a new open-source benchmark).
   - The instructions should contain the exact command and environment needed to run to reproduce the results. See the NeurIPS code and data submission guidelines (`https://nips.cc/public/guides/CodeSubmissionPolicy`) for more details.
   - The authors should provide instructions on data access and preparation, including how to access the raw data, preprocessed data, intermediate data, and generated data, etc.
   - The authors should provide scripts to reproduce all experimental results for the new proposed method and baselines. If only a subset of experiments are reproducible, they should state which ones are omitted from the script and why.
   - At submission time, to preserve anonymity, the authors should release anonymized versions (if applicable).
   - Providing as much information as possible in supplemental material (appended to the paper) is recommended, but including URLs to data and code is permitted.

6. **Experimental setting/details**

   Question: Does the paper specify all the training and test details (e.g., data splits, hyperparameters, how they were chosen, type of optimizer, etc.) necessary to understand the results?

   Answer: [Yes]

   Justification: Section 5 and Appendix D enumerate optimizer, batch-size, learning-rate schedules, client-fraction, and number of communication rounds for every experiment.

   Guidelines:

   - The answer NA means that the paper does not include experiments.
   - The experimental setting should be presented in the core of the paper to a level of detail that is necessary to appreciate the results and make sense of them.
   - The full details can be provided either with the code, in appendix, or as supplemental material.

7. **Experiment statistical significance**

   Question: Does the paper report error bars suitably and correctly defined or other appropriate information about the statistical significance of the experiments?

   Answer: [Yes]

   Justification: Table 3 list mean $\pm$ std over three random seeds.

   Guidelines:

- The answer NA means that the paper does not include experiments.
- The authors should answer "Yes" if the results are accompanied by error bars, confidence intervals, or statistical significance tests, at least for the experiments that support the main claims of the paper.
- The factors of variability that the error bars are capturing should be clearly stated (for example, train/test split, initialization, random drawing of some parameter, or overall run with given experimental conditions).
- The method for calculating the error bars should be explained (closed form formula, call to a library function, bootstrap, etc.)
- The assumptions made should be given (e.g., Normally distributed errors).
- It should be clear whether the error bar is the standard deviation or the standard error of the mean.
- It is OK to report 1-sigma error bars, but one should state it. The authors should preferably report a 2-sigma error bar than state that they have a 96% CI, if the hypothesis of Normality of errors is not verified.
- For asymmetric distributions, the authors should be careful not to show in tables or figures symmetric error bars that would yield results that are out of range (e.g. negative error rates).
- If error bars are reported in tables or plots, The authors should explain in the text how they were calculated and reference the corresponding figures or tables in the text.

8. **Experiments compute resources**

   Question: For each experiment, does the paper provide sufficient information on the computer resources (type of compute workers, memory, time of execution) needed to reproduce the experiments?

   Answer: [Yes]

   Justification: Appendix D states that tasks ran on a single NVIDIA RTX 3090 with 24 GB memory.

   Guidelines:

   - The answer NA means that the paper does not include experiments.
   - The paper should indicate the type of compute workers CPU or GPU, internal cluster, or cloud provider, including relevant memory and storage.
   - The paper should provide the amount of compute required for each of the individual experimental runs as well as estimate the total compute.
   - The paper should disclose whether the full research project required more compute than the experiments reported in the paper (e.g., preliminary or failed experiments that didn't make it into the paper).

9. **Code of ethics**

   Question: Does the research conducted in the paper conform, in every respect, with the NeurIPS Code of Ethics `https://neurips.cc/public/EthicsGuidelines`?

   Answer: [Yes]

   Justification: All datasets are publicly licensed, no personal data is processed, and the work advances communication-efficient FL without impacting protected groups.

   Guidelines:

   - The answer NA means that the authors have not reviewed the NeurIPS Code of Ethics.
   - If the authors answer No, they should explain the special circumstances that require a deviation from the Code of Ethics.
   - The authors should make sure to preserve anonymity (e.g., if there is a special consideration due to laws or regulations in their jurisdiction).

10. **Broader impacts**

    Question: Does the paper discuss both potential positive societal impacts and negative societal impacts of the work performed?

    Answer: [NA]

Justification: MAPO is a foundational optimisation technique; we judged its societal impact neutral and did not include a separate Broader-Impact section.

Guidelines:

- The answer NA means that there is no societal impact of the work performed.
- If the authors answer NA or No, they should explain why their work has no societal impact or why the paper does not address societal impact.
- Examples of negative societal impacts include potential malicious or unintended uses (e.g., disinformation, generating fake profiles, surveillance), fairness considerations (e.g., deployment of technologies that could make decisions that unfairly impact specific groups), privacy considerations, and security considerations.
- The conference expects that many papers will be foundational research and not tied to particular applications, let alone deployments. However, if there is a direct path to any negative applications, the authors should point it out. For example, it is legitimate to point out that an improvement in the quality of generative models could be used to generate deepfakes for disinformation. On the other hand, it is not needed to point out that a generic algorithm for optimizing neural networks could enable people to train models that generate Deepfakes faster.
- The authors should consider possible harms that could arise when the technology is being used as intended and functioning correctly, harms that could arise when the technology is being used as intended but gives incorrect results, and harms following from (intentional or unintentional) misuse of the technology.
- If there are negative societal impacts, the authors could also discuss possible mitigation strategies (e.g., gated release of models, providing defenses in addition to attacks, mechanisms for monitoring misuse, mechanisms to monitor how a system learns from feedback over time, improving the efficiency and accessibility of ML).

11. **Safeguards**

Question: Does the paper describe safeguards that have been put in place for responsible release of data or models that have a high risk for misuse (e.g., pretrained language models, image generators, or scraped datasets)?

Answer: [NA]

Justification: No new pretrained model or scraped dataset with misuse potential is released.

Guidelines:

- The answer NA means that the paper poses no such risks.
- Released models that have a high risk for misuse or dual-use should be released with necessary safeguards to allow for controlled use of the model, for example by requiring that users adhere to usage guidelines or restrictions to access the model or implementing safety filters.
- Datasets that have been scraped from the Internet could pose safety risks. The authors should describe how they avoided releasing unsafe images.
- We recognize that providing effective safeguards is challenging, and many papers do not require this, but we encourage authors to take this into account and make a best faith effort.

12. **Licenses for existing assets**

Question: Are the creators or original owners of assets (e.g., code, data, models), used in the paper, properly credited and are the license and terms of use explicitly mentioned and properly respected?

Answer: [Yes]

Justification: Each dataset and code baseline is cited, and the licenses are listed in the code, where they are used.

Guidelines:

- The answer NA means that the paper does not use existing assets.
- The authors should cite the original paper that produced the code package or dataset.

- The authors should state which version of the asset is used and, if possible, include a URL.
- The name of the license (e.g., CC-BY 4.0) should be included for each asset.
- For scraped data from a particular source (e.g., website), the copyright and terms of service of that source should be provided.
- If assets are released, the license, copyright information, and terms of use in the package should be provided. For popular datasets, `paperswithcode.com/datasets` has curated licenses for some datasets. Their licensing guide can help determine the license of a dataset.
- For existing datasets that are re-packaged, both the original license and the license of the derived asset (if it has changed) should be provided.
- If this information is not available online, the authors are encouraged to reach out to the asset's creators.

13. **New assets**

    Question: Are new assets introduced in the paper well documented and is the documentation provided alongside the assets?

    Answer: [NA]

    Justification: The work introduces no new dataset or model checkpoint; only source code is provided.

    Guidelines:

    - The answer NA means that the paper does not release new assets.
    - Researchers should communicate the details of the dataset/code/model as part of their submissions via structured templates. This includes details about training, license, limitations, etc.
    - The paper should discuss whether and how consent was obtained from people whose asset is used.
    - At submission time, remember to anonymize your assets (if applicable). You can either create an anonymized URL or include an anonymized zip file.

14. **Crowdsourcing and research with human subjects**

    Question: For crowdsourcing experiments and research with human subjects, does the paper include the full text of instructions given to participants and screenshots, if applicable, as well as details about compensation (if any)?

    Answer: [NA]

    Justification: Experiments are purely computational; no human subjects or crowd-work involved.

    Guidelines:

    - The answer NA means that the paper does not involve crowdsourcing nor research with human subjects.
    - Including this information in the supplemental material is fine, but if the main contribution of the paper involves human subjects, then as much detail as possible should be included in the main paper.
    - According to the NeurIPS Code of Ethics, workers involved in data collection, curation, or other labor should be paid at least the minimum wage in the country of the data collector.

15. **Institutional review board (IRB) approvals or equivalent for research with human subjects**

    Question: Does the paper describe potential risks incurred by study participants, whether such risks were disclosed to the subjects, and whether Institutional Review Board (IRB) approvals (or an equivalent approval/review based on the requirements of your country or institution) were obtained?

    Answer: [NA]

    Justification: No human-subject research was performed.

Guidelines:

- The answer NA means that the paper does not involve crowdsourcing nor research with human subjects.
- Depending on the country in which research is conducted, IRB approval (or equivalent) may be required for any human subjects research. If you obtained IRB approval, you should clearly state this in the paper.
- We recognize that the procedures for this may vary significantly between institutions and locations, and we expect authors to adhere to the NeurIPS Code of Ethics and the guidelines for their institution.
- For initial submissions, do not include any information that would break anonymity (if applicable), such as the institution conducting the review.

16. **Declaration of LLM usage**

Question: Does the paper describe the usage of LLMs if it is an important, original, or non-standard component of the core methods in this research? Note that if the LLM is used only for writing, editing, or formatting purposes and does not impact the core methodology, scientific rigorousness, or originality of the research, declaration is not required.

Answer: [NA]

Justification: No LLM was part of the method; any LLM assistance was limited to manuscript editing and is therefore outside the scope of the policy.

Guidelines:

- The answer NA means that the core method development in this research does not involve LLMs as any important, original, or non-standard components.
- Please refer to our LLM policy (`https://neurips.cc/Conferences/2025/LLM`) for what should or should not be described.